EUROPEAN ORGANIZATION FOR NUCLEAR RESEARCH

# Supplemental material: Medium-induced modification of groomed and ungroomed jet mass and angularities in Pb–Pb collisions at $\sqrt{s_{NN}} = 5.02$ TeV

ALICE Collaboration[*]

## Abstract

The ALICE Collaboration presents a new suite of jet substructure measurements in Pb–Pb and pp collisions at a center-of-mass energy per nucleon pair $\sqrt{s_{NN}} = 5.02$ TeV. These measurements provide access to the internal structure of jets via the momentum and angle of their constituents, probing how the quark–gluon plasma modifies jets, an effect known as jet quenching. Jet grooming additionally removes soft wide-angle radiation to enhance perturbative accuracy and reduce experimental uncertainties. We report the groomed and ungroomed jet mass $m_{\text{jet}}$ and jet angularities $\lambda_\alpha^\kappa$ using $\kappa = 1$ and $\alpha > 0$. Charged-particle jets are reconstructed at midrapidity using the anti-$k_{\text{T}}$ algorithm with $E$-scheme recombination and resolution parameter $R = 0.2$. This public note complements the publication of the same title with an explicit presentation of all the $m_{\text{jet}}$ and $\lambda_\alpha^\kappa$ results obtained using these data sets. A narrowing of the jet mass and angularity distributions in Pb–Pb collisions with respect to pp is observed and is enhanced for groomed results, confirming modification of the jet core. By using consistent jet definitions and kinematic cuts between the mass and angularities for the first time, previous inconsistencies in the interpretation of quenching measurements are resolved, rectifying a hurdle for understanding how jet quenching arises from first principles and highlighting the importance of a well-controlled baseline. These results are compared with a variety of theoretical models of jet quenching, providing constraints on jet energy-loss mechanisms in the quark–gluon plasma.

[*]See Appendix A for the list of collaboration members

# 1   Introduction

Collisions of ultra-relativistic heavy ions at the Large Hadron Collider (LHC) allow the study of bulk properties in quantum chromodynamics (QCD) at high temperature and density. These collisions produce a strongly-interacting state of matter called the quark–gluon plasma (QGP) [1, 2] where quarks and gluons are deconfined from nucleons. The hard scattering of two partons from these collisions forms collimated sprays of particles called jets. As they traverse the QGP, the partonic jets lose energy to the medium and their internal structure is modified, an effect known as jet quenching [3–7]. Consequently, jets can probe the structure and evolution of the QGP, and provide information about QGP transport properties, degrees of freedom, and the mechanisms for energy loss, as a function of momentum scale.

Jet substructure observables, which characterize the angular and transverse momentum distributions of the particles which constitute jets, can quantify these QGP quenching effects [8, 9]. For example, the jet invariant mass,

$$m_{\mathrm{jet}} \equiv \sqrt{E_{\mathrm{jet}}^2 - p_{\mathrm{jet}}^2},\tag{1}$$

where $E_{\mathrm{jet}}$ is the jet energy and $p_{\mathrm{jet}}$ its total momentum, has seen extensive experimental [10–20] and theoretical [21–24] study in recent years. The generalized jet angularities [25–29] are another class of such observables, defined as

$$\lambda_\alpha^\kappa \equiv \sum_{i \in \mathrm{jet}} \left( \frac{p_{\mathrm{T},i}}{p_\mathrm{T}^{\mathrm{ch\,jet}}} \right)^\kappa \left( \frac{\Delta R_i}{R} \right)^\alpha,\tag{2}$$

where $i$ runs over constituents in the jet, $p_\mathrm{T}$ designates transverse momentum, $R$ is the jet resolution parameter, and $\Delta R_i \equiv \sqrt{(y_{\mathrm{jet}} - y_i)^2 + (\varphi_{\mathrm{jet}} - \varphi_i)^2}$ gives the distance between the jet axis and its $i$th constituent in the rapidity ($y$) – azimuthal angle ($\varphi$) plane. The continuous parameters $\alpha$ and $\kappa$ define the specific observable, where the $\kappa = 1$ and $\alpha > 0$ configurations are infrared and collinear (IRC) safe [30].

Both $m_{\mathrm{jet}}$ and $\lambda_\alpha^\kappa$ characterize the jet radial energy profile, with a direct theoretical relation between them,

$$\lambda_2^1 = \left( \frac{m_{\mathrm{jet}}}{p_\mathrm{T}^{\mathrm{ch\,jet}} R} \right)^2 + \mathcal{O}[(\lambda_2^1)^2],\tag{3}$$

where $\lambda_2^1$ is also called the jet thrust [31], and the last term contains higher-order corrections in $m_{\mathrm{jet}}$ [32]. The jet thrust is also related to the jet girth [33], $g = \lambda_1^1 R$, with a smaller angular weighting $\alpha$. The ALICE collaboration measured $g$ and $m_{\mathrm{jet}}$ in Pb–Pb collisions during LHC Run 1 at nucleon–nucleon center-of-mass energy $\sqrt{s_{\mathrm{NN}}} = 2.76$ TeV, and compared the results to Monte Carlo models of pp collisions [11, 34]. Significant quenching modification was observed for $g$, while no significant modification was seen for $m_{\mathrm{jet}}$. Since $g$ and $m_{\mathrm{jet}}$ are theoretically related, this discrepancy was unexpected. These measurements differed in their ranges of $p_\mathrm{T}^{\mathrm{ch\,jet}}$, associated with quenching strength and nonperturbative dependence, as well as the angular weighting $\alpha$, associated with momentum broadening, which both could account for the discrepancy.

This public note presents angularities for the 10% most central Pb–Pb collisions at $\sqrt{s_{\mathrm{NN}}} = 5.02$ TeV. A recent measurement of IRC-safe angularities in pp collisions at identical center-of-mass energy is used as a no-quenching baseline [35]. We preserve the convenient notation $\lambda_\alpha \equiv \lambda_\alpha^1$ from this measurement, and compare these angularities with new measurements of $m_{\mathrm{jet}}$ using the same pp and Pb–Pb collision data, using equivalent $R$ for the first time to address the girth–mass inconsistency. The results are reported for background-subtracted charged-particle jets with transverse momenta of $40 < p_\mathrm{T}^{\mathrm{ch\,jet}} < 150$ GeV/$c$, extending the results published in Ref. [36]. These results at higher $p_\mathrm{T}^{\mathrm{ch\,jet}}$ extend the kinematic reach of previous measurements and probe the strength of jet-medium interactions at varying energy scales.

Soft drop grooming [37] is employed to remove soft wide-angle radiation from jets, minimizing the nonperturbative dependence of $m_{\mathrm{jet}}$ and $\lambda_\alpha$. Systematically varying $p_\mathrm{T}^{\mathrm{ch\,jet}}$, $\alpha$, $R$, and grooming for each

observable provides coherent constraints on models of jet quenching.

## 2 Experimental setup and data sets

A description of the ALICE detector and its performance can be found in Refs. [38, 39]. The pp data set used in this analysis was collected in 2017 during LHC Run 2 at $\sqrt{s} = 5.02$ TeV. A minimum bias (MB) trigger was used, which required a coincidence of hits in V0A and V0C detectors, covering pseudorapidity ranges of $2.8 < \eta < 5.1$ and $-3.7 < \eta < -1.7$, respectively [40]. The Pb–Pb data set was collected in 2018 during LHC Run 2 at $\sqrt{s_{NN}} = 5.02$ TeV. A centrality trigger that selects the 0–10% most central events, based on the multiplicity of produced particles in the forward V0 counters, was used [41, 42]. The event selection includes a primary vertex selection, where the primary vertex is required to be unique for the event and to be within $\pm 10$ ($\pm 1$) cm from the center of the detector in the longitudinal (transverse) direction. Beam-induced background events are removed using the timing information of the V0 detectors and, in Pb–Pb collisions, two neutron Zero Degree Calorimeters located $\pm 112.5$ m along the beam axis from the center of the detector. Pileup is rejected based on multiple reconstructed vertices and tracking selections [39]. After these selections, the pp data sample contains 870 million events and corresponds to an integrated luminosity of $18.0 \pm 0.4$ nb$^{-1}$ [43]. The corresponding Pb–Pb data sample contains 91.2 million events in 0-10% most central collisions, corresponding to an integrated luminosity of $0.119 \pm 0.003$ nb$^{-1}$ [44].

This analysis uses charged particle tracks reconstructed using information from both the Time Projection Chamber (TPC) [45] and the Inner Tracking System (ITS) [46]. Two types of tracks are defined: global tracks and complementary tracks. Global tracks are required to include at least one hit in the silicon pixel detector (SPD) comprising the first two layers of the ITS and to satisfy multiple tracking criteria. Complementary tracks are all those satisfying all the selection criteria of global tracks except for the request of a point in the SPD. They are refitted using the primary vertex to constrain their trajectory in order to preserve a good momentum resolution, especially at high $p_T$. Including this second class of tracks ensures approximately uniform azimuthal acceptance, while preserving similar transverse-momentum $p_T$ resolution to tracks with SPD hits. Tracks with $0.15 < p_T < 100$ GeV/$c$ are accepted over pseudorapidity $|\eta| < 0.9$ and azimuthal angle $0 < \varphi < 2\pi$. The track $p_T$ selection has no effect on jets with $p_T^{ch\,jet} < 100$ GeV/$c$ and has a negligible effect on jets with $100 < p_T^{ch\,jet} < 150$ GeV/$c$.

The instrumental performance of the detector is estimated with a model of the ALICE detector and its response to particles using GEANT3 [47]. The tracking efficiency in pp collisions, as estimated with a simulation performed with PYTHIA8 Monash 2013 [48] for the event generation and using the GEANT3 [47] transport code for propagating particles through the simulated ALICE apparatus simulation, is approximately 67% at track $p_T = 0.15$ GeV/$c$, and rises to approximately 84% at $p_T = 1$ GeV/$c$, and remains above 75% at higher $p_T$. Studies of the centrality dependence of the tracking efficiency in a HIJING [49] simulation demonstrate that the tracking efficiency is approximately 2% lower in 0–10% central Pb–Pb collisions compared to pp collisions, independent of track $p_T$. The momentum resolution $\sigma(p_T)/p_T$ is estimated from the covariance matrix of the track fit [39], and is approximately 1% at track $p_T = 1$ GeV/$c$ and 4% at $p_T = 50$ GeV/$c$.

## 3 Analysis method

### 3.1 Jet reconstruction

Jets are reconstructed from charged-particle tracks with FastJet 3.3.3 [50] using the anti-$k_T$ algorithm with $E$-scheme recombination for resolution parameter $R = 0.2$ [51, 52]. Despite track-based observables being collinear-unsafe [53], they offer greater momentum and angular precision than calorimeter-based observables. The $\pi^\pm$ meson mass is assumed for all jet constituents. For pp collisions, all reconstructed

jets in the range $5 < p_T^{ch\,jet} < 200$ GeV/$c$ are analyzed. Jets in heavy-ion collisions have a large uncorre-lated background contribution due to fluctuations in the underlying event (UE), owing to the large number of soft, thermally-produced particles from the QGP. In ALICE, the UE contribution is quantified through the transverse momentum density per unit area, $\rho$, which is on average 146 GeV/$c$ in central (0-10%) collisions. To reduce this thermal background, this measurement uses the event-by-event constituent subtraction method, which corrects the overall $p_T^{ch\,jet}$ and its substructure simultaneously by subtracting energy constituent by constituent [54, 55]. The constituent subtraction method works by adding mass-less, negligible "ghosts" to the event over the entire acceptance whose transverse momentum is very small and negative. The ghosts and particles are then combined based on how close they are to each other, as defined by

$$\Delta R = (p_T)^{\alpha} \cdot \sqrt{(\eta - \eta_g)^2 + (\varphi - \varphi_g)^2} \tag{4}$$

where $\eta_g$ and $\varphi_g$ are the $\eta$ and $\varphi$ of the ghosts, $p_T$ is the transverse momentum of the particle, and $\alpha$ is a parameter that can be varied. Particles and ghosts with less than zero total momentum are removed from the event. The maximum recombination distance $R_{max}$ specifies how close the particles and ghosts must be to be considered a match. The values $R_{max} = 0.1$ and $\alpha = 0$ are chosen, which yields a corrected charged-particle jet transverse momentum $p_T^{ch\,jet}$ with minimal smearing. After background subtraction, the measured range is $40 < p_T^{ch\,jet} < 200$ GeV/$c$, which is used in the unfolding procedure (see Sect. 3.2) and corrected to the final reported range of $40 < p_T^{ch\,jet} < 150$ GeV/$c$. The jet axis is required to be within the fiducial volume of the TPC, $|\eta_{jet}| < 0.9 - R = 0.7$, where $\eta_{jet}$ is the jet pseudorapidity. Jets containing a track with $p_T^{track} > 100$ GeV/$c$ are rejected in order to optimize the overall jet momentum resolution. This rejection has a negligible effect on jets with $p_T^{ch\,jet} < 150$ GeV/$c$.

The jet reconstruction performance is studied via a Monte Carlo (MC) approach, by comparing PYTHIA8 generated jets at "truth level" (before the particles undergo interactions with the detector) to those at "de-tector level" (after the ALICE GEANT3 detector simulation). In pp collisions two collections of jets are constructed: pp truth level (PYTHIA truth) and pp detector level (PYTHIA with detector simula-tion). The detector-level jets are then geometrically matched with truth-level jets within $\Delta R < 0.6\,R$, and required to be a unique match. To create the MC sample for Pb–Pb collisions, PYTHIA events are em-bedded into 0–10% centrality Pb–Pb measured events. A truth-level jet from PYTHIA is then assigned with an associated "combined" jet, consisting of a jet constructed from PYTHIA detector level tracks with tracks from the Pb–Pb data. Since the tracking efficiency in Pb–Pb data is roughly 2% worse than in pp, 2% of all tracks are also randomly rejected from the events at detector-level before applying jet reconstruction to account for this difference. Three collections of jets are therefore defined: pp truth level and pp detector level, in the same way as in pp collisions, and combined level. A scheme of jet matching is used where the "combined" jet is matched geometrically to the nearest pp detector-level jet, requiring that the jets are within $\Delta R < 0.6\,R$ and that the combined jet contains at least 50% of the total $p_T^{track}$ of the pp detector-level jet, implicitly enforcing uniqueness. Additionally, the pp detector-level jet is matched to its corresponding pp truth-level jet in the same way as was done for the jets in pp collisions.

For the groomed jet observables, we perform soft drop grooming [37], in which the jet is re-clustered with the Cambridge-Aachen algorithm with resolution parameter $R$. The jet is then declustered starting from the largest-angle splitting, where each splitting in the declustered sequence is defined by

$$z \equiv \frac{p_{T,subleading}}{p_{T,leading} + p_{T,subleading}}. \tag{5}$$

If the so-called *soft drop condition* is not satisfied by a particular splitting, meaning that

$$z \leq z_{cut}\theta^{\beta}, \tag{6}$$

where the angle $\theta$ is defined by

$$\theta \equiv \frac{\Delta R}{R} \equiv \frac{\sqrt{\Delta y^2 + \Delta \varphi^2}}{R}, \tag{7}$$

where $\Delta y$ ($\Delta \varphi$) is the difference between the jet and contituent rapidity (azimuthal angle), and $z_{\mathrm{cut}}$ and $\beta$ are free parameters of the grooming algorithm, then the softer branch is dropped, and we proceed to the next splitting in the harder branch. If the soft drop condition is satisfied, meaning Eq. 6 is *not* true, then the grooming procedure is concluded, with all remaining constituents defining the groomed jet. The groomed jet angularity $\lambda_{\alpha,\mathrm{g}}$ and groomed jet mass $m_{\mathrm{jet,g}}$ are then defined according to the remaining jet constituents, using Eqs. 1–2 as before. The value of $\lambda_{\alpha,\mathrm{g}}$ is calculated using the ungroomed $p_{\mathrm{T}}^{\mathrm{ch\,jet}}$ and calculating $\Delta R_i$ with respect to the ungroomed jet axis, as the groomed jet remnants are a property of the original ungroomed jet.

Local background fluctuations in a heavy-ion environment can result in an incorrect splitting being identified by the grooming algorithm, in which the reconstructed splitting is unrelated to a hard process. In order to address this issue, this measurement has been performed by requiring the jet to have a splitting where the softer branch carries 20% or more of the groomed transverse momentum (i.e., $z_{\mathrm{cut}} = 0.2$) independent of the angle of the splitting (i.e., $\beta = 0$), which improves the efficiency of tagging the first hard splitting in the large background of Pb–Pb collisions, as compared to milder grooming conditions such as $z_{\mathrm{cut}} = 0.1$ [56]. Additionally, by measuring jets with a small resolution parameter ($R = 0.2$ instead of $R = 0.4$), the magnitude of these prong-mistagging effects was further decreased, since the collinear jet fragmentation enhances the fraction of signal jet energy with respect to the background energy density. Prong mistagging due to the residual background effects ranges from approximately 5% up to 15% at lower $p_{\mathrm{T}}$ [57]. The impact of the residual background contribution is quantified in Sect. 4.

### 3.2 Unfolding

The reconstructed $p_{\mathrm{T}}^{\mathrm{ch\,jet}}$ along with the groomed and ungroomed $\lambda_\alpha$ and $m_{\mathrm{jet}}$ differ from their true values due to tracking inefficiency, particle-material interactions, and track $p_{\mathrm{T}}$ resolution. Moreover, in Pb–Pb collisions, background fluctuations significantly smear the reconstructed distributions. To account for these effects, MC pp events are simulated with the PYTHIA8 generator [48] using the Monash 2013 tune and the GEANT3 model [47] for the particle transport in the ALICE detector material. Jets are reconstructed from these simulated events following the procedure described above (Sec. 3.1). A 4D response matrix (RM) is then constructed that describes the detector and background response in $p_{\mathrm{T}}^{\mathrm{ch\,jet}}$ and $\lambda_\alpha$ or $m_{\mathrm{jet}}$,

$$\mathrm{RM}\left(p_{\mathrm{T,\,det}}^{\mathrm{ch\,jet}},\ p_{\mathrm{T,\,truth}}^{\mathrm{ch\,jet}},\ \lambda_{\alpha,\mathrm{det}},\ \lambda_{\alpha,\mathrm{truth}}\right), \tag{8}$$

where the subscript 'det' refers to detector-level quantities in the case of pp collisions, or the combined-level jet after embedding and background subtraction in the case of Pb–Pb collisions, and the subscript 'truth' refers to the truth-level (generator-level) quantities. Equation 8 holds analogously for $m_{\mathrm{jet}}$ and the groomed counterparts. A 2D unfolding is performed in $p_{\mathrm{T}}^{\mathrm{ch\,jet}}$ and $\lambda_\alpha$ or $m_{\mathrm{jet}}$ using the iterative Bayesian unfolding algorithm [58] as implemented in the RooUnfold software package [59].

In order to reject jets formed from the random combination of tracks emanated from the thermal background produced in Pb–Pb collisions, a lower limit of $p_{\mathrm{T,\,det}}^{\mathrm{ch\,jet}} > 40$ GeV/$c$ is enforced on the data that is input to the unfolding. No such limitation is imposed on $p_{\mathrm{T,\,truth}}^{\mathrm{ch\,jet}}$ during the unfolding process. The distributions after unfolding are then corrected for the kinematic efficiency, defined as the efficiency of reconstructing a "true" jet at a particular $p_{\mathrm{T,\,truth}}^{\mathrm{ch\,jet}}$ value given a reconstructed jet $p_{\mathrm{T,\,det}}^{\mathrm{ch\,jet}}$ range. This inefficiency results from background effects, smearing from the soft drop threshold $z_{\mathrm{cut}}$, and detector effects smearing $p_{\mathrm{T}}^{\mathrm{ch\,jet}}$ out of the selected range. Since the final observables are normalized per jet, the kinematic efficiency only affects the shape of the distribution. The kinematic efficiency is 70% or higher in all cases for $p_{\mathrm{T}}^{\mathrm{ch\,jet}} > 60$ GeV/$c$. For the lowest $40 < p_{\mathrm{T}}^{\mathrm{ch\,jet}} < 60$ GeV/$c$ bin, where kinematic efficiency corrections are larger, the shape of the efficiency correction is verified by repeating the unfolding procedure with varied jet shape assumptions. This is done by using several MC event generators, including PYTHIA8, Herwig 7 [60, 61], and JEWEL [62], along with a fast detector simulation which emulates

the tracking efficiency and track $p_T$ resolution of the ALICE detector. The number of untagged jets is included in the unfolding procedure as an additional bin adjacent to the lower edge of the $\lambda_\alpha$ and $m_{jet}$ distributions (in iterative Bayesian unfolding, the arrangement of the bins is immaterial). The number of iterations, which sets the strength of regularization, is chosen by checking that the unfolding closure tests (described below) are successful. This results in the optimal number of iterations ranging from 5 to 15, with the larger number of iterations offering increased accuracy in the lowest $p_T^{ch\,jet}$ bin.

To validate the performance of the unfolding procedure, refolding tests are performed, in which the RM is multiplied by the unfolded solution and compared to the original detector-level spectrum. The unfolding is required to obtain reasonable convergence, which is evaluated by checking that successive iterations produce smaller changes in the distributions. Three types of closure tests are also performed. A "statistical" closure test smears detector-level MC by measured uncertainties on the data and unfolds the smeared distribution by the nominal RM and compares the resulting spectrum to the truth-level MC which is expected. Examples of the convergence and statistical closure tests are shown in Fig. 1. A "shape" closure test is also performed, where the shape of the input spectrum is modified to account for the fact that the actual distribution may be different than the MC input spectrum. The "prior" closure test instead modifies the shape of the RM to account for differences in the bias of the MC shape. In all cases, closure is achieved within statistical uncertainties. A thermal closure test is additionally performed for the Pb–Pb analyses to quantify the sensitivity of the final result to combinatorial jets and background splittings. This consists of redoing the entire analysis on combined events containing a PYTHIA event and a thermal background, in which combined-level jets are clustered from the combination of PYTHIA detector-level particles and thermal background particles. The background is modeled by generating $N$ particles with $p_T$ taken from a Gamma distribution,

$$f_\Gamma(p_T; \beta) \propto p_T e^{-p_T/\beta}, \tag{9}$$

where $N$ and $\beta$ are fixed to roughly fit the $\delta p_T$ distribution (the difference truth- and combined-level $p_T^{ch\,jet}$) for $R = 0.2$ jets in Pb–Pb data [63]. This background model was verified to describe the subleading prong purity to percent-level accuracy. The test consisted of constructing the combined detector-level jet spectrum, building the RM, unfolding the combined jets, and comparing the resulting spectrum to the truth-level PYTHIA spectrum. Since the background does not have any jet component, this test is able to quantify the extent to which the analysis procedure recovers the signal distribution and is not contaminated by background. Due to a residual background contamination, slight non-closure is observed in some distributions and is therefore incorporated as a systematic uncertainty, discussed further in Sect. 4.

## 4   Systematic uncertainties

The systematic uncertainties for observables reported in this note are estimated from the uncertainty on the tracking efficiency, the unfolding procedure, the background subtraction procedure, the generator model-dependence, and any non-closure in a thermal closure test. Tables 1 and 2 summarize the systematic uncertainty contributions for $\lambda_\alpha$ and $m_{jet}$ in Pb–Pb collisions, as well as the systematic uncertainty contributions for their soft drop groomed counterparts $\lambda_{\alpha,g}$ and $m_{jet,g}$. Table 3 correspondingly gives the systematic uncertainty contributions to $m_{jet}$ in pp collisions.[1] All sources of systematic uncertainty contribute significantly in certain regions of the measured observables. The total systematic uncertainty is calculated as the quadratic sum of all of the individual systematic uncertainties described below.

The systematic uncertainties tend to be largest at low $p_T^{ch\,jet}$, where tracking efficiency effects are more significant compared to the overall $p_T^{ch\,jet}$, the distributions are closer to the detector-level cuts, and there is greater modeling uncertainty due to increased nonperturbative dependence. Systematic uncertainties

---

[1]The systematic uncertainty contributions for $\lambda_\alpha$ in pp collisions are reported in Ref. [35].
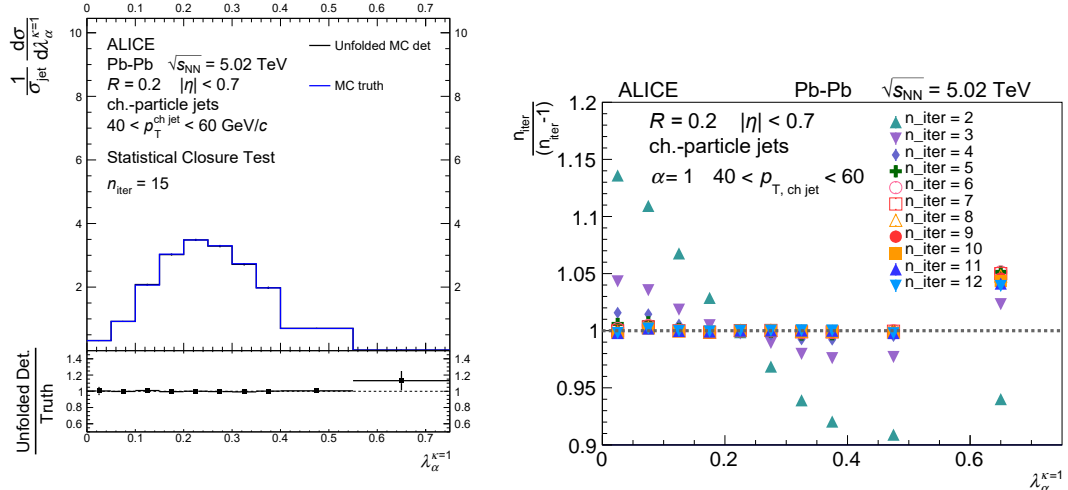
**Fig. 1:** *Left:* example of a statistical closure test; *right:* example of an unfolding convergence test, both for the jet girth in Pb–Pb with $40 < p_{\rm T}^{\rm ch\,jet} < 60$ GeV/$c$. In both cases, the rightmost (highest) $\lambda_\alpha$ bin is included only for statistical considerations and is truncated from the reported distributions.

are typically lower in the groomed distributions, where removal of soft radiation reduces these effects. For the Pb–Pb observables, the highest $100 < p_{\rm T}^{\rm ch\,jet} < 150$ GeV/$c$ bin has no pp baseline, so it was binned more finely than the lower $p_{\rm T}^{\rm ch\,jet}$ bins; as a result, the tails of the distribution are more sensitive to systematic fluctuations, and enhanced values are observed for some systematic uncertainty contributions.

In general, correcting for unmeasured tracks is a major effect of the unfolding procedure. The systematic uncertainty due to the tracking efficiency uncertainty is evaluated using random rejection of tracks before jet finding. The tracking efficiency uncertainty is estimated to be 3% in pp [2] and 3–5% in Pb–Pb collisions, depending on track $p_{\rm T}$, based on variations in the track selection criteria and on the ITS–TPC track-matching efficiency uncertainty. Since the nominal Pb–Pb RM randomly rejects 2% of all tracks to account for the worsened tracking efficiency in Pb–Pb data as compared to pp, the varied response matrix in total randomly rejects approximately 2% more than these calculated values. This response matrix is then used to unfold the same measured data as used in the final result. This variation is compared to the nominal result, with the differences in each bin taken as the tracking efficiency uncertainty. Since the tracking efficiency uncertainty is symmetric, the uncertainties on the jet distributions which result from this subtraction procedure are also taken to be symmetric.

In application of unfolding, the underlying systematic uncertainty is due to the regularization. In order to quantify the size of this uncertainty, several systematic variations are performed on the unfolding procedure, which assign a shape uncertainty arising from the regularization:

– **Variation of the regularization parameter** $n_{\rm iter}$ by $\pm 2$ units (for $\lambda_\alpha$ and $\lambda_{\alpha,\rm g}$) or $\pm 1$ unit (for $m_{\rm jet}$ and $m_{\rm jet,g}$). The average deviation of these two variations is taken as the systematic uncertainty.

– **Variation of the prior** by scaling the shape by $p_{\rm T}^{\pm 0.5} \times [1 \pm 0.5(2\lambda_\alpha - 1)]$ (for $\lambda_\alpha$) or by $p_{\rm T}^{\pm 0.5} \times N_{\rm counts}^{\pm 0.1}$ (for $m_{\rm jet}$). These scaling functions were determined by approximating the differences between detector-level simulation and data. For $m_{\rm jet}$, it is also mandated that $0.5 \leq N_{\rm counts}^{\pm 0.1} \leq 1.5$, else it is set to the boundary values as to not over-modulate the tails of distributions. These variations are chosen since they vary the prior quite dramatically to demonstrate a broad range of independence on the prior, via an effect that would be reasonably expected in differing calculations (smoothing or sharpening of the distributions). The maximum of the $\pm$ case is chosen for

---

[2] The measurements of $\lambda_\alpha$ in pp collisions instead use a more generous 4% tracking efficiency uncertainty assumption, as the results were finalized before the more recent 3% estimation was completed.

each bin and used as the systematic uncertainty due to the prior in that bin.

- **Variation of the binning** of the observable. An alternate binning is constructed with slightly finer and/or coarser granularity than the main result, by adding and/or reducing the number of bins by 1 or 2. This is performed for both the data and RM. The unfolding is then repeated, and the difference with respect to the nominal result is taken as the systematic uncertainty.

- **Variation of the truncation** of $p_{\mathrm{T,\,det}}^{\mathrm{ch\,jet}}$. The lower and upper $p_{\mathrm{T,\,det}}^{\mathrm{ch\,jet}}$ limits are truncated by 5 and 50 GeV/$c$, respectively, also taking into account the kinematic efficiency considerations. For the lowest $40 < p_{\mathrm{T}}^{\mathrm{ch\,jet}} < 60$ GeV/$c$ bin, the upper $p_{\mathrm{T,\,det}}^{\mathrm{ch\,jet}}$ limit is truncated by a more liberal 80 GeV/$c$. Similar to the binning variation, the unfolding is again repeated using the varied data and RM, and the difference with respect to the nominal result is taken as the systematic uncertainty.

Since each of these procedures comprise independent measurements of the same underlying systematic uncertainty in the regularization, the total unfolding systematic uncertainty is taken as the standard deviation of these variations, $\sqrt{\sum_{i=1}^{N} \sigma_i^2 / N}$, where $\sigma_i$ is the systematic uncertainty due to a single variation. In this case, $N = 4$, as there are four unfolding uncertainties calculated for these analyses.

To quantify the model-dependence of using PYTHIA 8 [48] to build the RM, alternate RMs are built using different MC generators. In particular, RMs are produced using Herwig 7 [60, 61] and JEWEL [62] (for Pb–Pb) using an identical binning and the same cuts as the nominal PYTHIA RM. To apply detector effects to the alternate MC events, a fast detector simulation is used, which applies tracking efficiency rejections and $p_{\mathrm{T}}$ smearing according to the GEANT3-estimated performance, both as a function of $p_{\mathrm{T}}^{\mathrm{track}}$. This simulation was validated on truth-level PYTHIA by comparing to PYTHIA with the full GEANT3 simulation, with agreement to the few-percent-level. In order to make equitable comparisons, both PYTHIA and the alternate MC events are run through this fast simulation, and the bin-by-bin differences are calculated in the final unfolded distributions, comparing the PYTHIA response to that from the alternate MCs. The average of the differences (for all variations) is taken as a systematic uncertainty.

In Pb–Pb analyses, background subtraction via iterative constituent subtraction introduces a bias in the observed distributions, since it implicitly makes a choice of how much to subtract the soft particles compared to hard particles, as well as their angular distributions. To estimate the size of the corresponding systematic uncertainty, the $R_{\mathrm{max}}$ parameter is varied generously from "undersubtraction" ($R_{\mathrm{max}} = 0.05$) to "oversubtraction" ($R_{\mathrm{max}} = 0.5$), around the nominal value of $R_{\mathrm{max}} = 0.1$. The maximum deviation of these two variations is taken as the systematic uncertainty.

As mentioned above, any non-closure in the thermal closure test is addressed by the addition of a thermal non-closure systematic uncertainty. The thermal closure test for each of the distributions is converted into a percentage of non-closure, and the statistical uncertainty is 'subtracted' from the nominal ratio in order to minimize covariance with the statistical uncertainties introduced by the smearing procedure in the unfolding. Specifically, the non-closure uncertainty is approximated from these ratios as

$$\sigma_{\mathrm{total}}^2 \approx \sigma_{\mathrm{stat}}^2 + \sigma_{\mathrm{non\text{-}closure}}^2, \tag{10}$$

thereby requiring that $\sigma_{\mathrm{total}} > \sigma_{\mathrm{stat}}$, or else it is assumed that reasonable closure is observed for that bin, in which case the thermal non-closure uncertainty is set to 0. As before, this bin-by-bin uncertainty is taken as being symmetric on each individual reported data point.

Each of the systematic uncertainties outlined above is assumed to be independent, and therefore they are summed in quadrature to obtain the total bin-by-bin systematic uncertainty. The liberal assumption of independence is intended to capture any missing components of the systematic uncertainty that were not addressed in the above methodologies.[3] The dominant systematic uncertainties are typically due to

---

[3] A more detailed procedure would involve reconstructing a covariance matrix for each of the variations, although this is nontrivial; therefore, the covariances between these systematic uncertainties are neglected.

uncertainty on the tracking efficiency and the dependence of unfolding on the model which is used to generate the RM.

| Pb–Pb | Relative uncertainty (%) | | | | | |
|---|---|---|---|---|---|---|
| $p_{\mathrm{T}}^{\mathrm{ch\,jet}}$ (GeV/$c$) | Trk. eff. | Unfolding | Generator | Therm. clos. | Bkgd. sub. | Total |
| $\lambda_1$ | | | | | | |
| 40 - 60 | 1–20% | 0–4% | 2–8% | 0–4% | 0–8% | 4–24% |
| 60 - 80 | 1–9% | 0–2% | 1–3% | 0–2% | 3–13% | 3–16% |
| 80 - 100 | 2–6% | 0–3% | 1–4% | 0–3% | 2–8% | 4–11% |
| 100 - 150 | 2–76% | 0–3% | 1–5% | 0–5% | 2–10% | 7–77% |
| $\lambda_{1,\mathrm{g}}$ ($z_{\mathrm{cut}} = 0.2, \beta = 0$) | | | | | | |
| 40 - 60 | 0–5% | 1–8% | 3–12% | 0–4% | 0–9% | 4–18% |
| 60 - 80 | 0–6% | 0–4% | 0–8% | 0–4% | 1–8% | 2–11% |
| 80 - 100 | 1–4% | 2–3% | 1–10% | 0–4% | 1–7% | 3–14% |
| 100 - 150 | 1–10% | 1–3% | 1–8% | 0–9% | 0–11% | 7–17% |
| $\lambda_{1.5}$ | | | | | | |
| 40 - 60 | 1–12% | 0–6% | 1–8% | 0–1% | 1–9% | 4–16% |
| 60 - 80 | 1–8% | 0–2% | 1–3% | 0–3% | 2–12% | 3–15% |
| 80 - 100 | 2–9% | 0–2% | 2–8% | 0–3% | 3–9% | 4–14% |
| 100 - 150 | 7–47% | 0–2% | 0–8% | 0–7% | 0–15% | 8–48% |
| $\lambda_{1.5,\mathrm{g}}$ ($z_{\mathrm{cut}} = 0.2, \beta = 0$) | | | | | | |
| 40 - 60 | 0–10% | 1–12% | 2–11% | 0–2% | 1–18% | 3–26% |
| 60 - 80 | 0–6% | 0–2% | 0–8% | 0–4% | 2–8% | 3–11% |
| 80 - 100 | 0–4% | 1–3% | 2–8% | 0–4% | 0–12% | 5–11% |
| 100 - 150 | 3–9% | 1–7% | 1–10% | 1–7% | 1–12% | 6–20% |
| $\lambda_2$ | | | | | | |
| 40 - 60 | 0–11% | 0–3% | 1–5% | 0–3% | 3–7% | 5–14% |
| 60 - 80 | 0–9% | 1–3% | 0–4% | 0–2% | 3–12% | 3–16% |
| 80 - 100 | 1–9% | 0–2% | 1–9% | 0–1% | 1–7% | 3–12% |
| 100 - 150 | 0–28% | 0–3% | 1–9% | 0–10% | 0–12% | 6–29% |
| $\lambda_{2,\mathrm{g}}$ ($z_{\mathrm{cut}} = 0.2, \beta = 0$) | | | | | | |
| 40 - 60 | 1–6% | 0–4% | 0–11% | 0–3% | 1–9% | 3–16% |
| 60 - 80 | 0–6% | 0–3% | 2–9% | 0–3% | 2–9% | 3–12% |
| 80 - 100 | 0–4% | 0–3% | 2–10% | 0–3% | 2–7% | 4–14% |
| 100 - 150 | 0–10% | 1–4% | 0–10% | 0–7% | 3–8% | 8–17% |
| $\lambda_3$ | | | | | | |
| 40 - 60 | 0–9% | 0–7% | 0–6% | 0–2% | 2–11% | 5–17% |
| 60 - 80 | 0–10% | 0–3% | 1–4% | 0–3% | 2–9% | 3–12% |
| 80 - 100 | 1–7% | 0–2% | 1–5% | 0–2% | 3–9% | 4–12% |
| 100 - 150 | 2–17% | 0–3% | 0–9% | 0–3% | 2–12% | 3–21% |
| $\lambda_{3,\mathrm{g}}$ ($z_{\mathrm{cut}} = 0.2, \beta = 0$) | | | | | | |
| 40 - 60 | 2–7% | 0–6% | 2–10% | 0–4% | 0–8% | 3–15% |
| 60 - 80 | 2–6% | 1–4% | 2–11% | 0–4% | 1–8% | 4–14% |
| 80 - 100 | 0–3% | 1–3% | 2–11% | 0–3% | 0–9% | 3–16% |
| 100 - 150 | 5–12% | 2–4% | 1–9% | 1–6% | 1–9% | 6–18% |

**Table 1:** Summary of systematic uncertainties on the Pb–Pb measurements of $\lambda_\alpha$ and $\lambda_{\alpha,\mathrm{g}}$. The ranges correspond to the minimum and maximum systematic uncertainties obtained.

| Pb–Pb | Relative uncertainty (%) | | | | | |
|---|---|---|---|---|---|---|
| $p_{\mathrm{T}}^{\mathrm{ch\,jet}}$ (GeV/$c$) | Trk. eff. | Unfolding | Generator | Therm. clos. | Bkgd. sub. | Total |
| $m_{\mathrm{jet}}$ | | | | | | |
| 40 - 60 | 1–8% | 1–8% | 1–16% | 0–24% | 1–4% | 2–30% |
| 60 - 80 | 2–13% | 1–8% | 2–20% | 0–3% | 2–11% | 6–28% |
| 80 - 100 | 2–11% | 1–6% | 1–11% | 0–1% | 2–9% | 3–19% |
| 100 - 150 | 2–26% | 0–6% | 2–15% | 1–10% | 2–12% | 3–33% |
| $m_{\mathrm{jet,g}}$ ($z_{\mathrm{cut}} = 0.2$, $\beta = 0$) | | | | | | |
| 40 - 60 | 0–5% | 1–9% | 1–13% | 0–25% | 0–14% | 3–28% |
| 60 - 80 | 0–6% | 2–7% | 1–9% | 0–7% | 1–10% | 2–16% |
| 80 - 100 | 1–6% | 3–8% | 1–6% | 0–2% | 3–6% | 3–12% |
| 100 - 150 | 1–9% | 3–8% | 2–11% | 1–16% | 1–8% | 5–22% |

**Table 2:** Summary of systematic uncertainties on the Pb–Pb measurements of $m_{\mathrm{jet}}$ and $m_{\mathrm{jet,g}}$. The ranges correspond to the minimum and maximum systematic uncertainties obtained.

| pp | Relative uncertainty (%) | | | |
|---|---|---|---|---|
| $p_{\mathrm{T}}^{\mathrm{ch\,jet}}$ (GeV/$c$) | Trk. eff. | Unfolding | Generator | Total |
| $m_{\mathrm{jet}}$ | | | | |
| 40 - 60 | 1–8% | 1–6% | 0–20% | 2–22% |
| 60 - 80 | 2–16% | 0–7% | 1–20% | 3–26% |
| 80 - 100 | 0–11% | 1–8% | 1–11% | 2–17% |
| $m_{\mathrm{jet,g}}$ ($z_{\mathrm{cut}} = 0.2$, $\beta = 0$) | | | | |
| 40 - 60 | 0–6% | 1–28% | 0–13% | 3–28% |
| 60 - 80 | 0–18% | 2–18% | 1–16% | 2–30% |
| 80 - 100 | 2–8% | 5–9% | 0–8% | 5–13% |

**Table 3:** Summary of systematic uncertainties on the pp measurements. The ranges correspond to the minimum and maximum systematic uncertainties obtained. All values correspond to $z_{\mathrm{cut}} = 0.2$ unless otherwise noted.

## 5 Results

We report the $\lambda_\alpha$ and $m_{\text{jet}}$ distributions both with and without soft drop grooming with $z_{\text{cut}} = 0.2$ and $\beta = 0$ in bins of charged-jet transverse momentum $p_{\text{T}}^{\text{ch jet}}$ between 40 and 150 GeV/$c$ in central (0–10%) Pb–Pb collisions and between 40 and 100 GeV/$c$ in pp collisions. The measurements are reported using jet resolution (radius) parameter $R = 0.2$. The observable $O$ distributions (where $O$ is either $\lambda_\alpha$ or $m_{\text{jet}}$) are reported as self-normalized differential cross sections,

$$\frac{1}{\sigma}\frac{\mathrm{d}\sigma}{\mathrm{d}O} \equiv \frac{1}{N_{\text{jets}}}\frac{\mathrm{d}N_{\text{jets}}}{\mathrm{d}O} \text{ (ungroomed)}, \quad \text{or} \quad \frac{1}{\sigma_{\text{inc}}}\frac{\mathrm{d}\sigma}{\mathrm{d}O_{\text{g}}} \equiv \frac{1}{N_{\text{jets}}}\frac{\mathrm{d}N_{\text{gr jets}}}{\mathrm{d}O_{\text{g}}} \text{ (groomed)}, \tag{11}$$

where $N_{\text{jets}}$ is the number of inclusive jets within a given $p_{\text{T}}^{\text{ch jet}}$ range and $\sigma$ is the corresponding cross section. For the groomed case, some jets are removed by the grooming procedure ("untagged"), and therefore two different quantities are defined: $N_{\text{gr jets}}$, the number of jets which have at least one splitting satisfying the SD condition, and $N_{\text{jets}}$, the total number of inclusive jets, with both $N_{\text{gr jets}}$ and $N_{\text{jets}}$ being within the given $p_{\text{T}}^{\text{ch jet}}$ range. $N_{\text{jets}}$ is corrected from the raw data by including the number of untagged jets as an extra bin in the unfolding procedure. $\sigma_{\text{inc}}$ is the cross section corresponding to the latter inclusive quantity. For the ungroomed case, $\sigma = \sigma_{\text{inc}}$, so the redundant label is dropped. It is useful to normalize the groomed differential cross section by the number of inclusive jets since the groomed jet angularities are a property of the inclusively-measured jet population and are thus typically normalized as such in theoretical calculations [64].

Results for the ungroomed and SD-groomed jet angularities $\lambda_\alpha$ with $\alpha = 1$ (girth) are shown in Figs. 2–5, for $\alpha = 1.5$ in Figs. 6–9, for $\alpha = 2$ (thrust) in Figs. 10–13, and for $\alpha = 3$ in Figs. 14–17. The same are shown for the groomed and ungroomed jet mass $m_{\text{jet}}$ in Figs. 18–21. The Pb–Pb result is shown in the center panels along with the respective models, while the pp baselines are given in the left panel along with the corresponding model baselines. The superposition of the pp and Pb–Pb distributions along with the Pb–Pb/pp ratio, which quantifies the quenching modification, is shown in the right panels. The highest $100 < p_{\text{T}}^{\text{ch jet}} < 150$ GeV/$c$ bin does not have a baseline result from pp, so only the Pb–Pb result is reported.

The fraction of jets that do not contain a splitting that passes the Soft Drop condition ($f_{\text{tagged}}$) ranges from 10% to 12%. The differences in these tagging rates between pp and Pb–Pb are at most 2%. Since these differences between pp and Pb–Pb collisions are small, the measured distributions are approximately self-normalized, and therefore any modifications in Pb–Pb compared to pp can change the shape of the distribution, but keep the integral approximately the same.
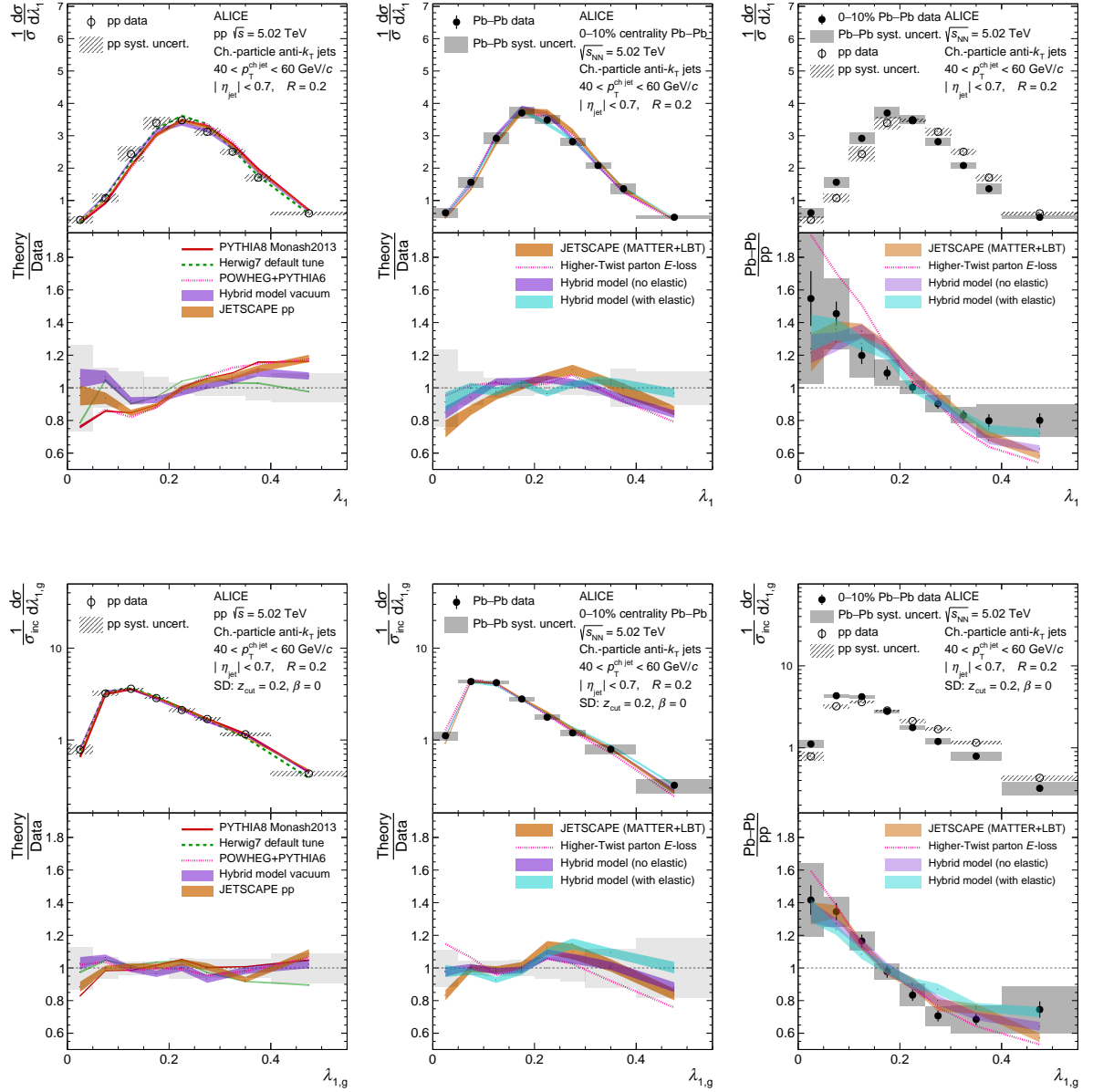
**Fig. 2:** ALICE measurement of ungroomed (top) and SD groomed (bottom) $\lambda_1$ for $R = 0.2$ charged-particle jets in pp (left) and Pb–Pb (middle) collisions at $\sqrt{s_{\text{NN}}} = 5.02$ TeV for $40 < p_{\text{T}}^{\text{ch jet}} < 60$ GeV/$c$ as compared to models. The ratio of Pb–Pb to pp is also shown (right), which quantifies the substructure modifications from quenching. The pp result is taken from Ref. [35].
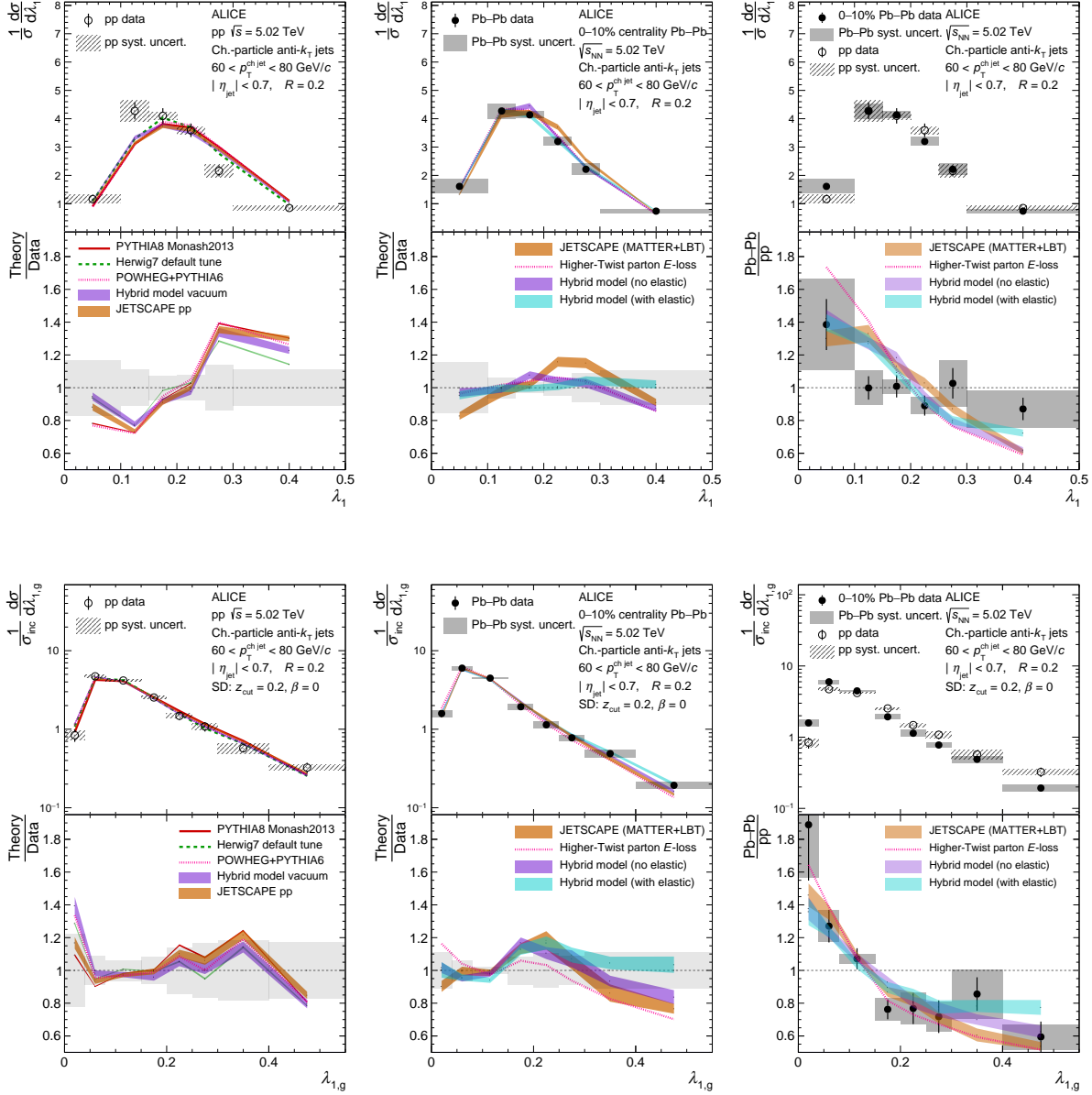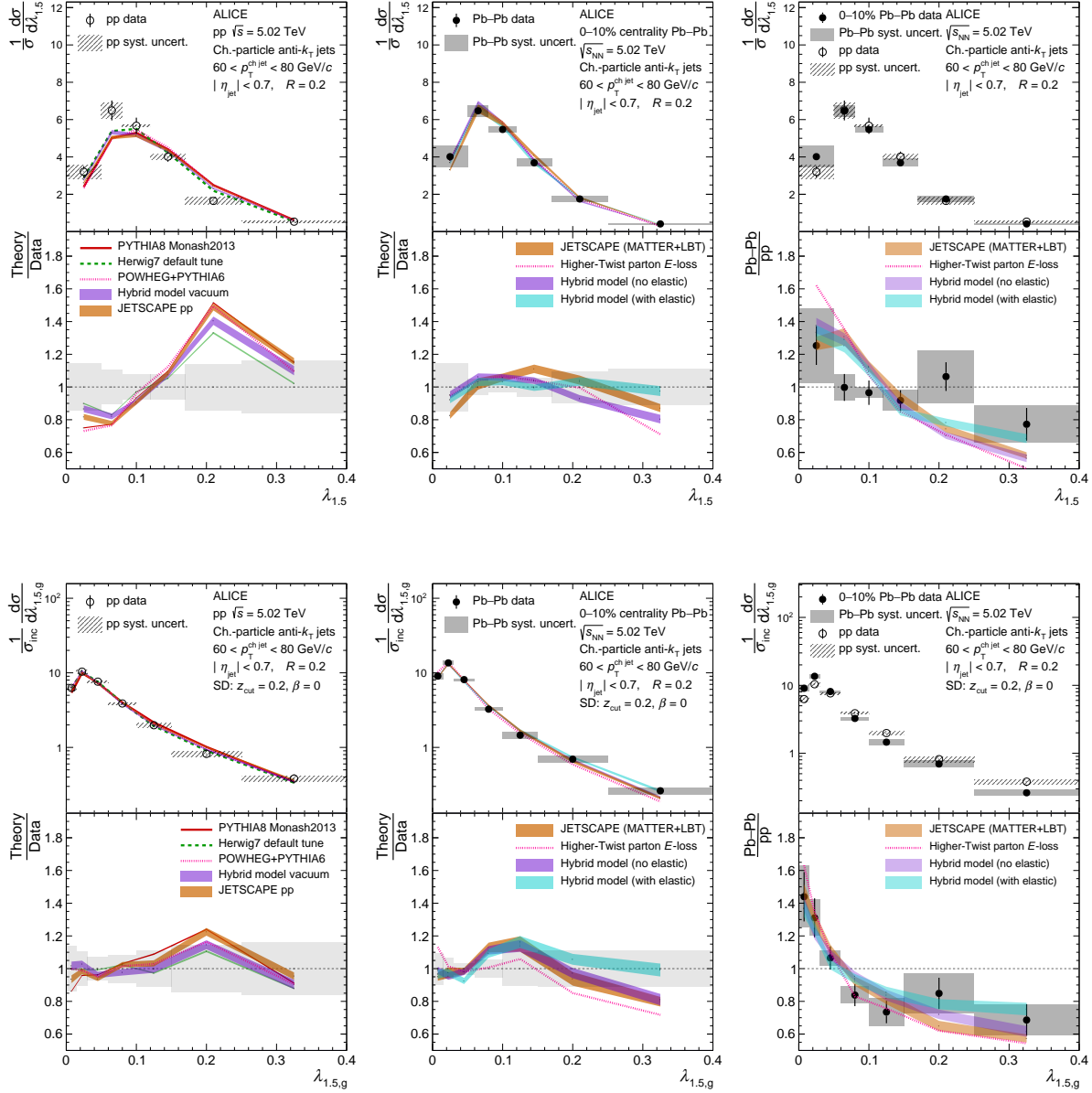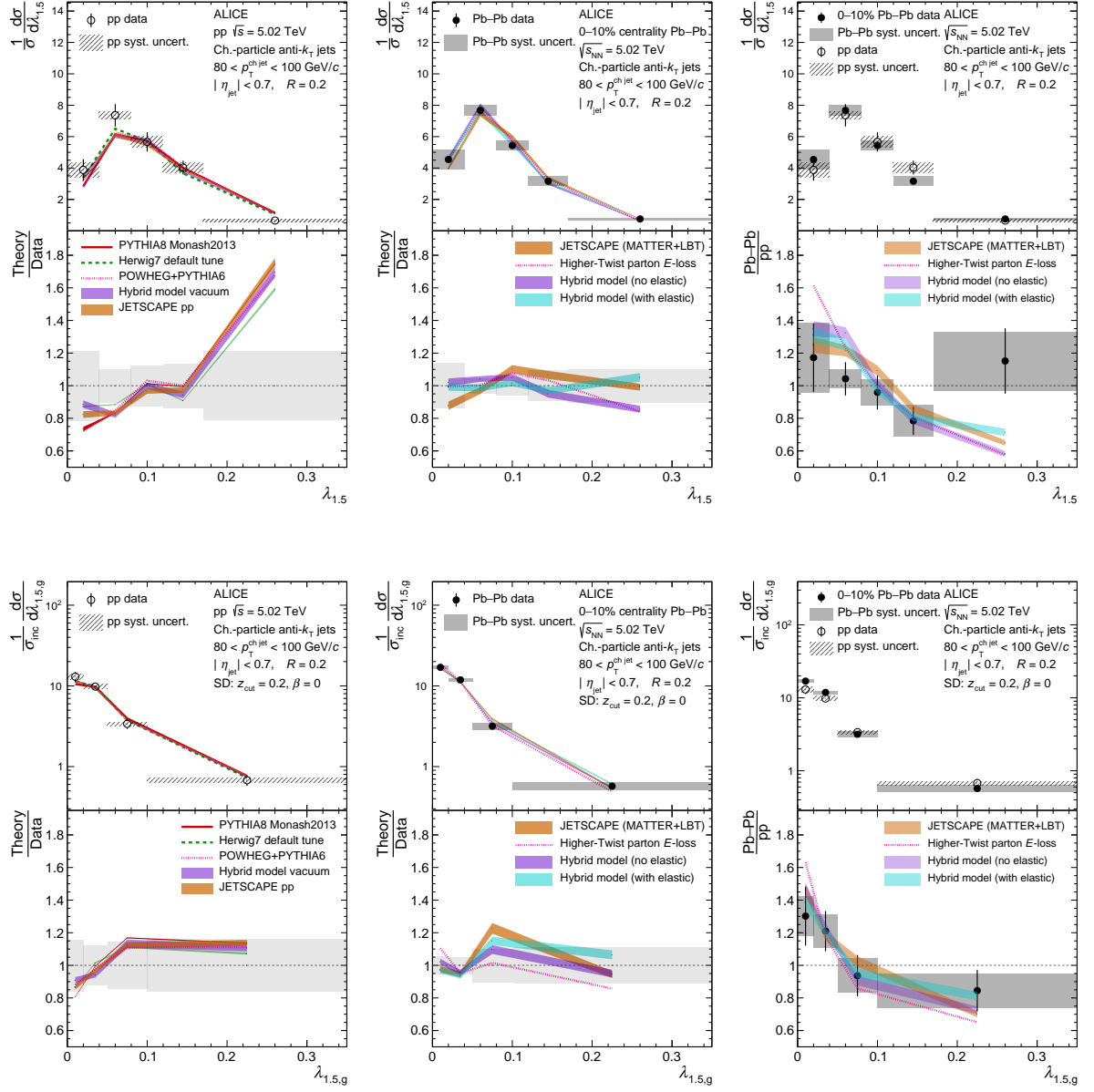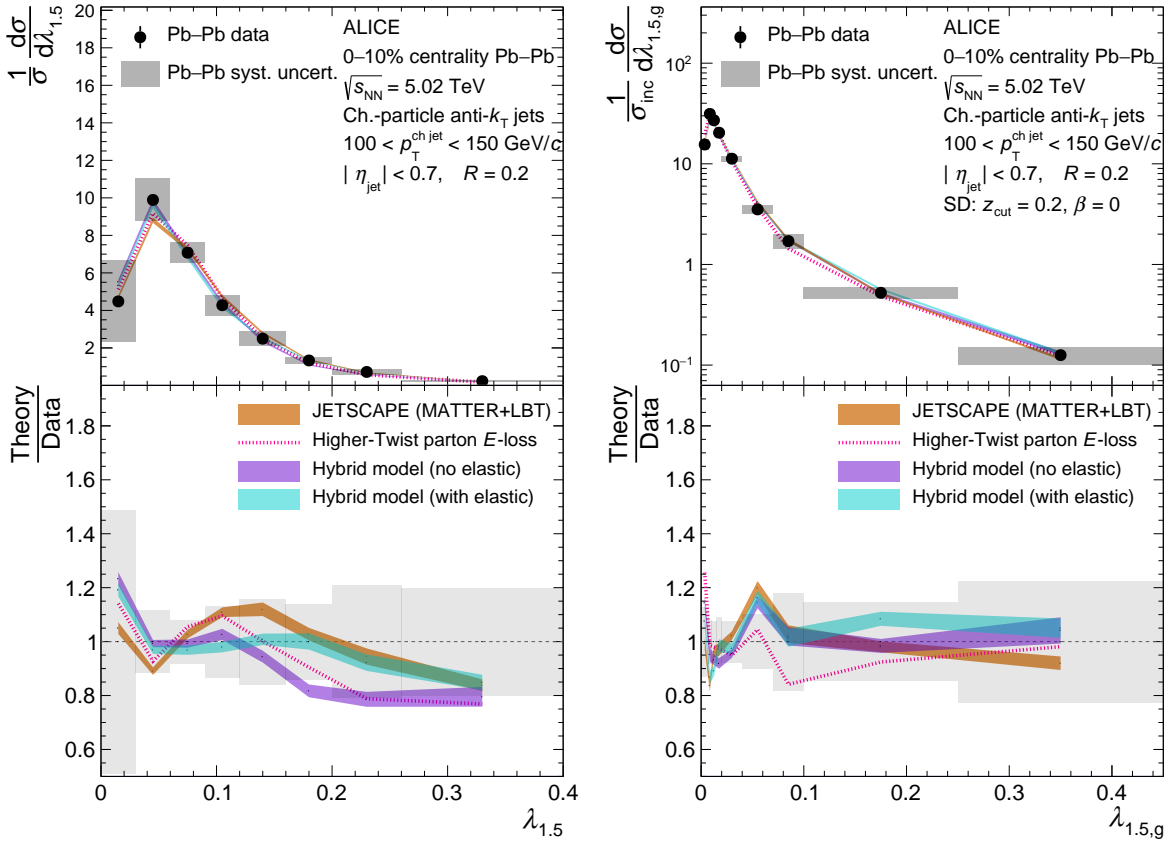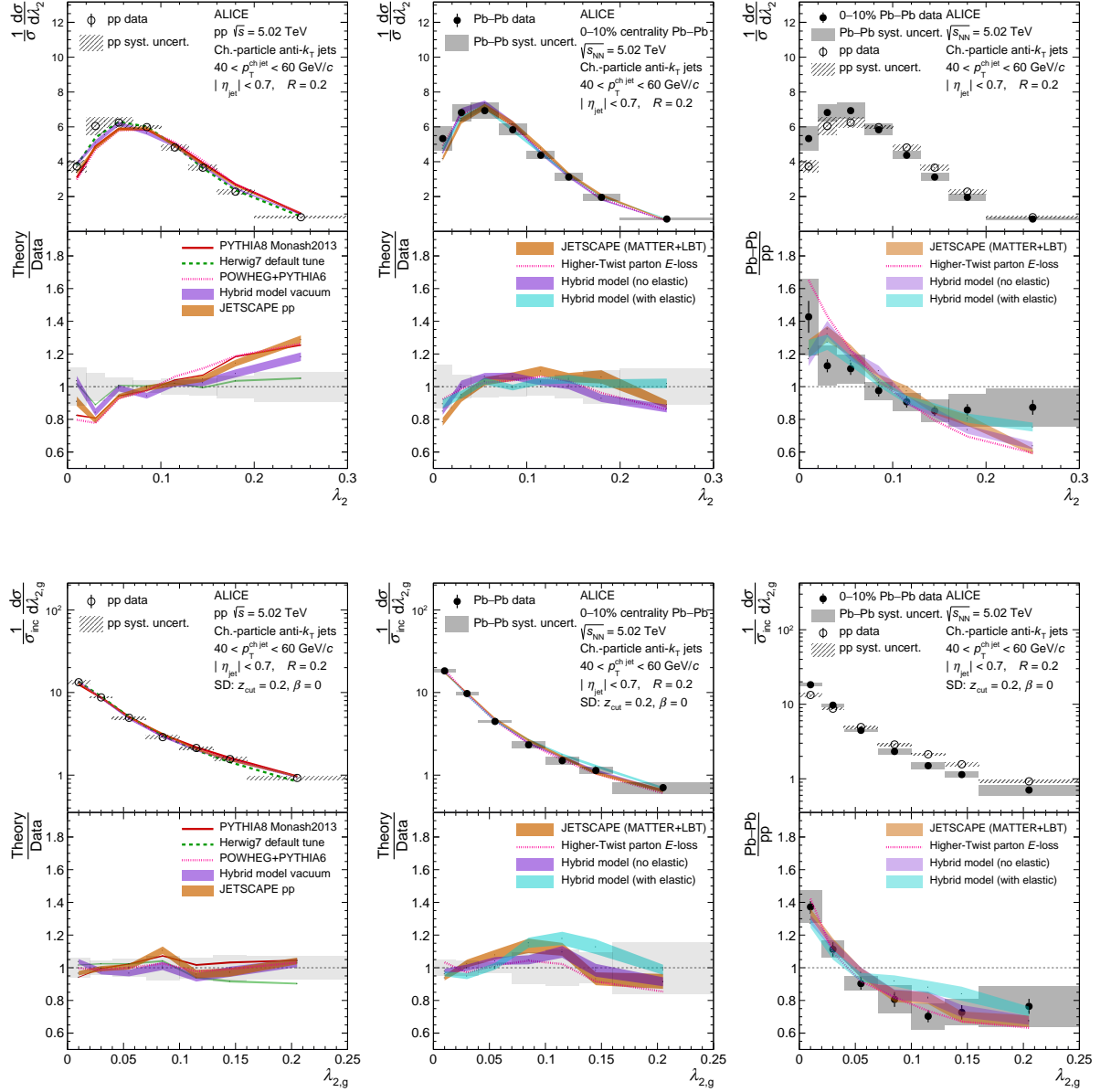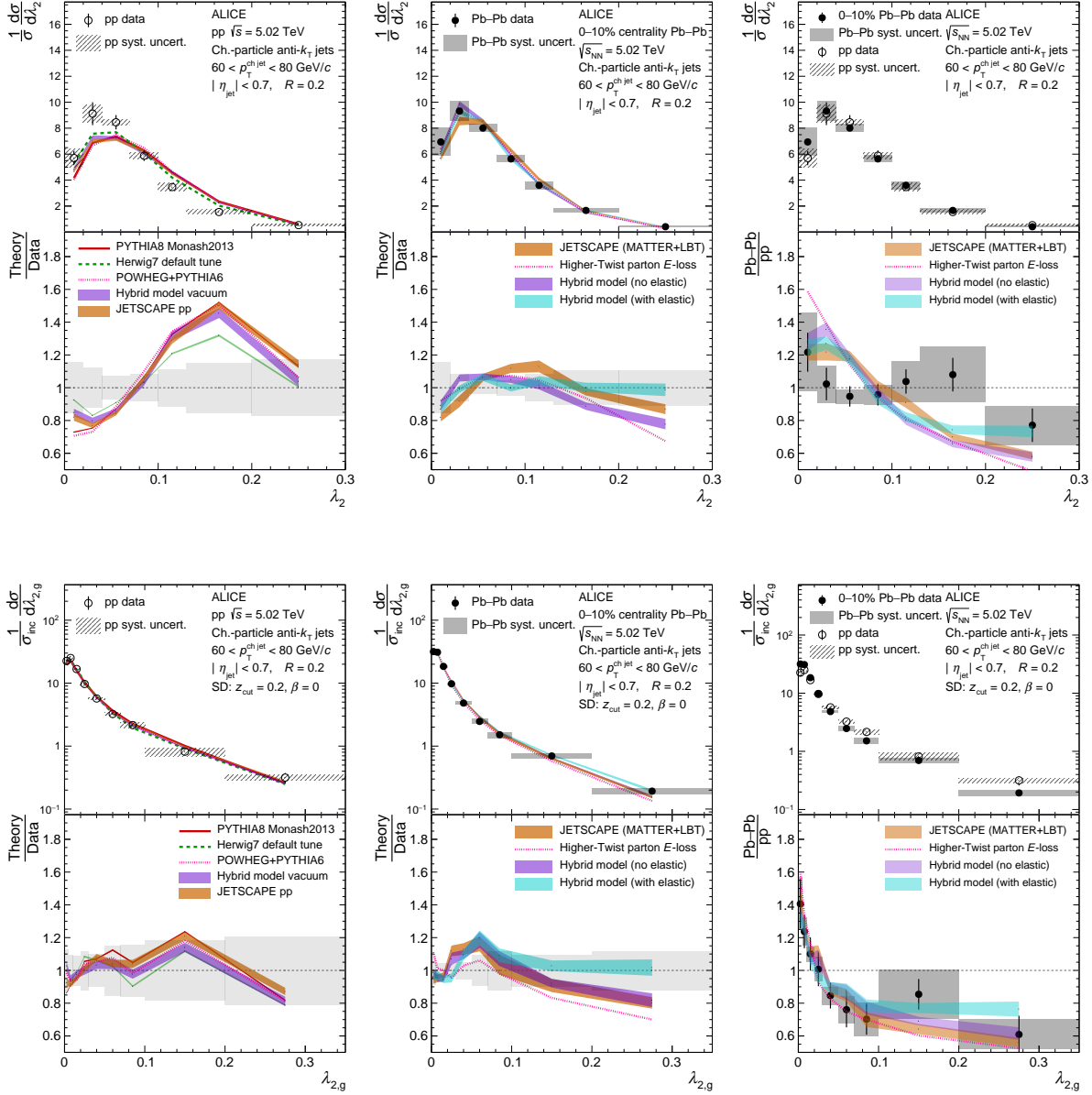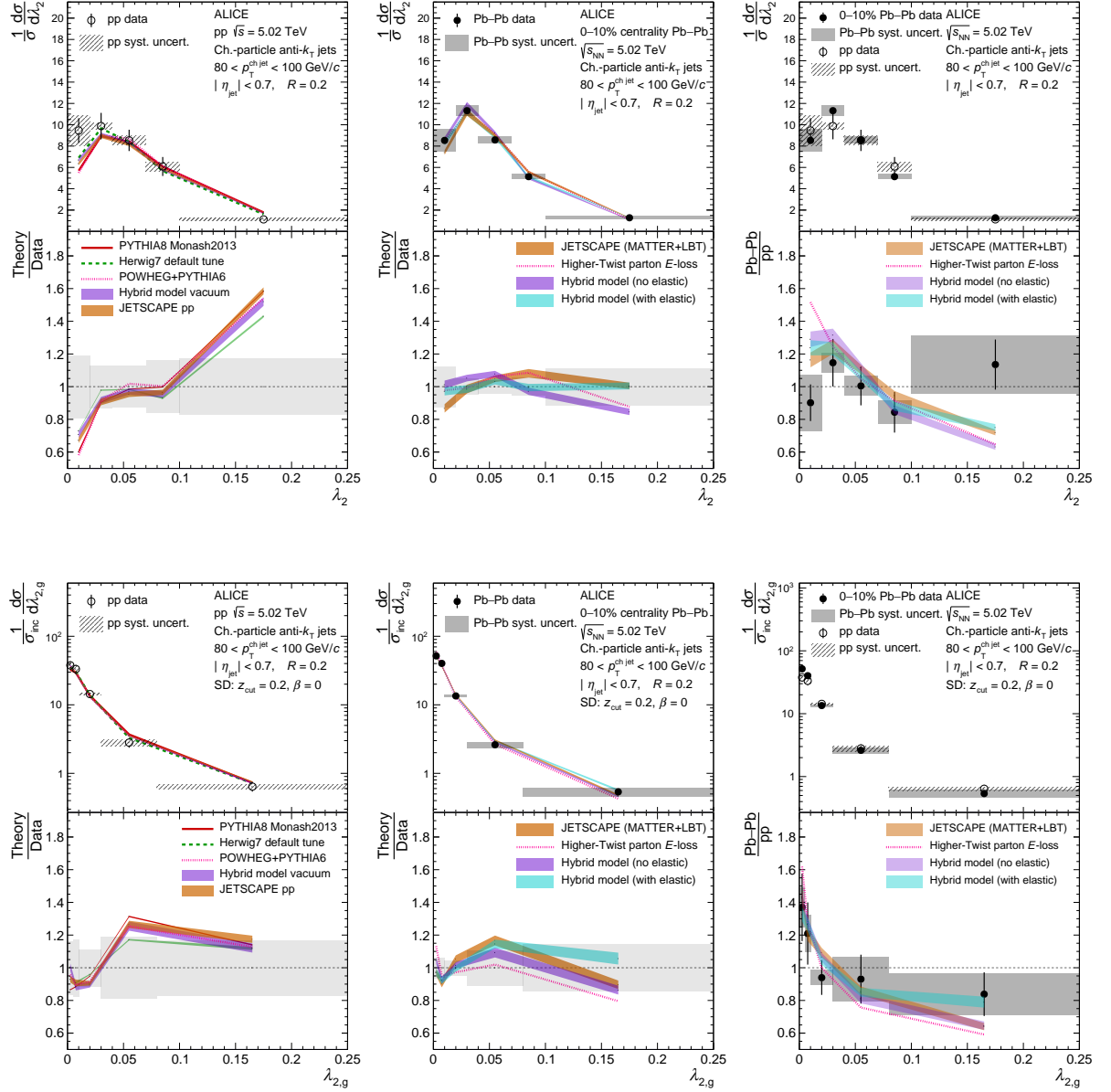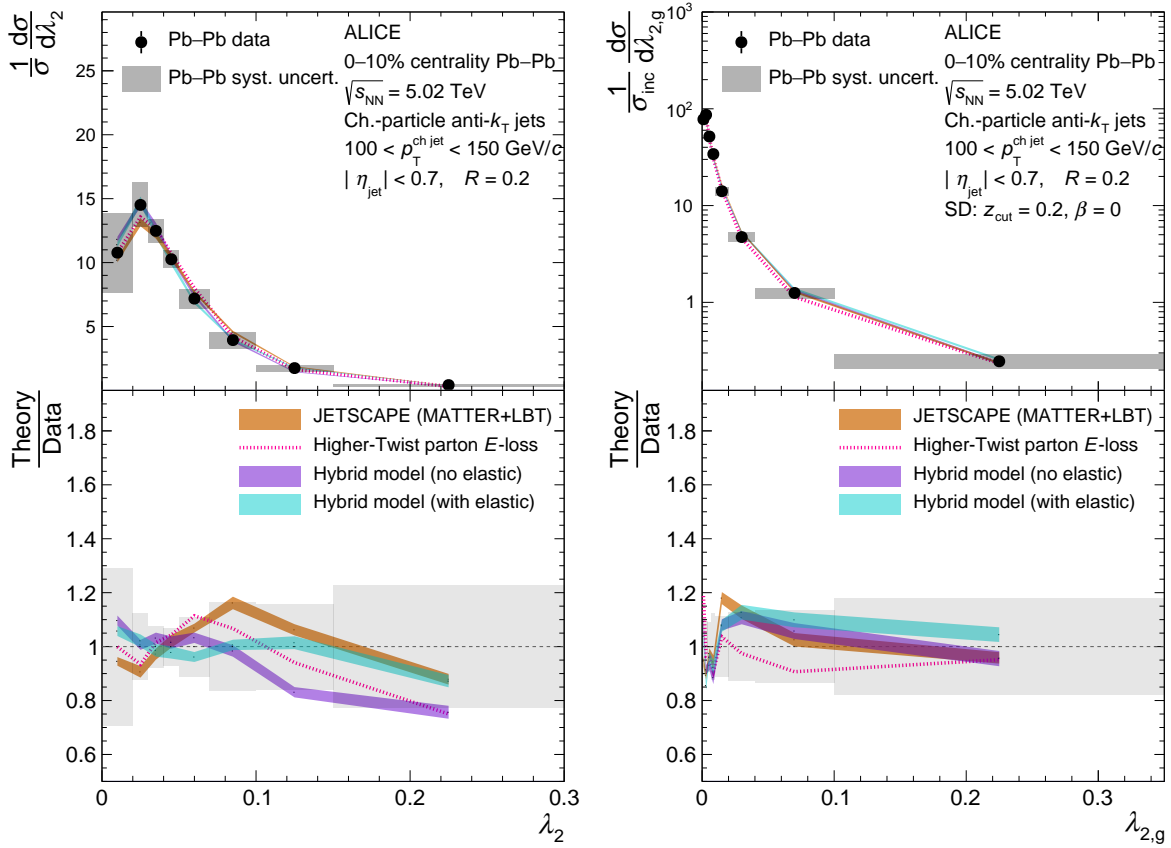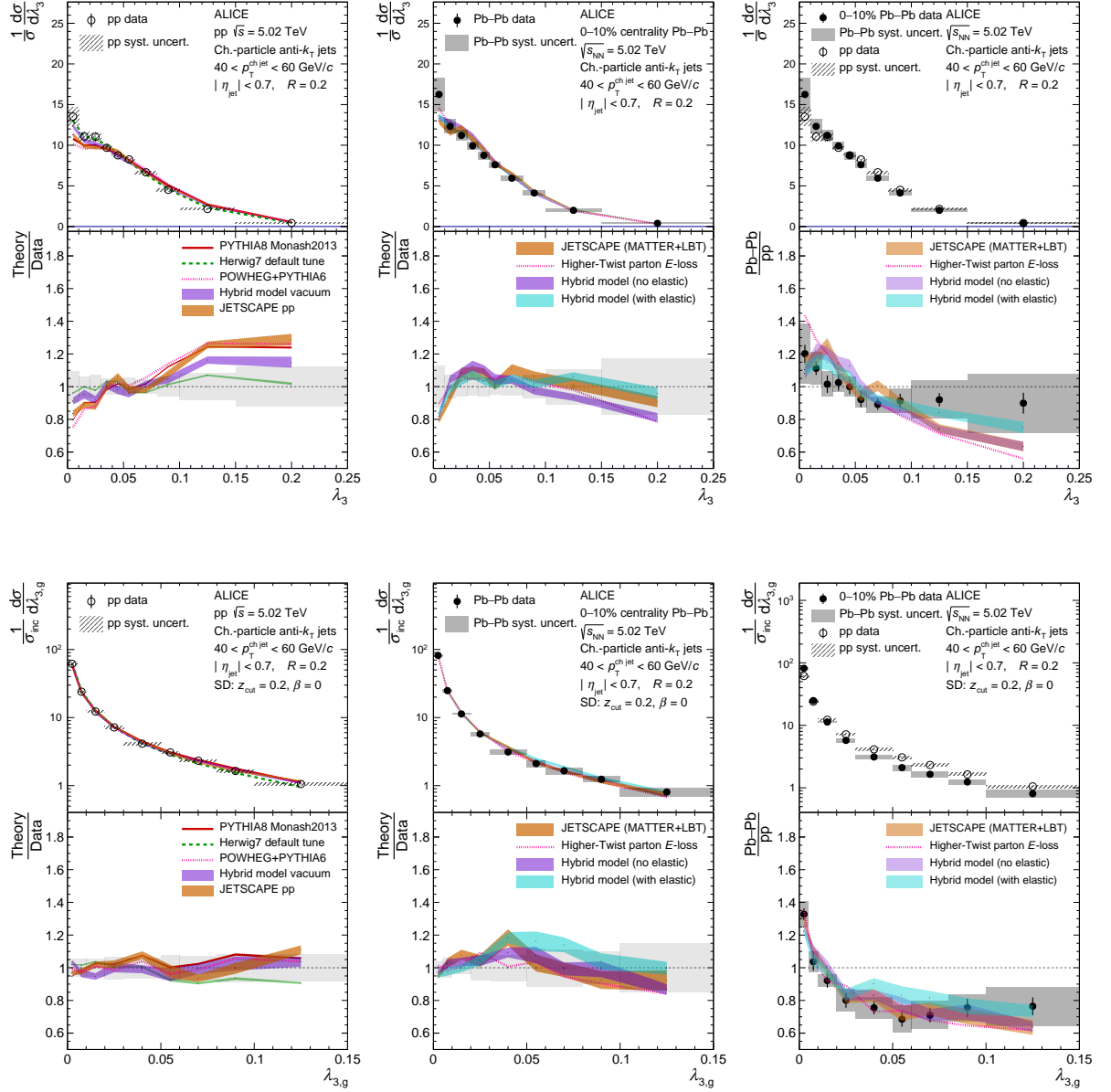
**Fig. 3:** ALICE measurement of ungroomed (top) and SD groomed (bottom) $\lambda_1$ for $R = 0.2$ charged-particle jets in pp (left) and Pb–Pb (middle) collisions at $\sqrt{s_{NN}} = 5.02$ TeV for $60 < p_T^{ch\,jet} < 80$ GeV/$c$ as compared to models. The ratio of Pb–Pb to pp is also shown (right), which quantifies the substructure modifications from quenching. The pp result is taken from Ref. [35].
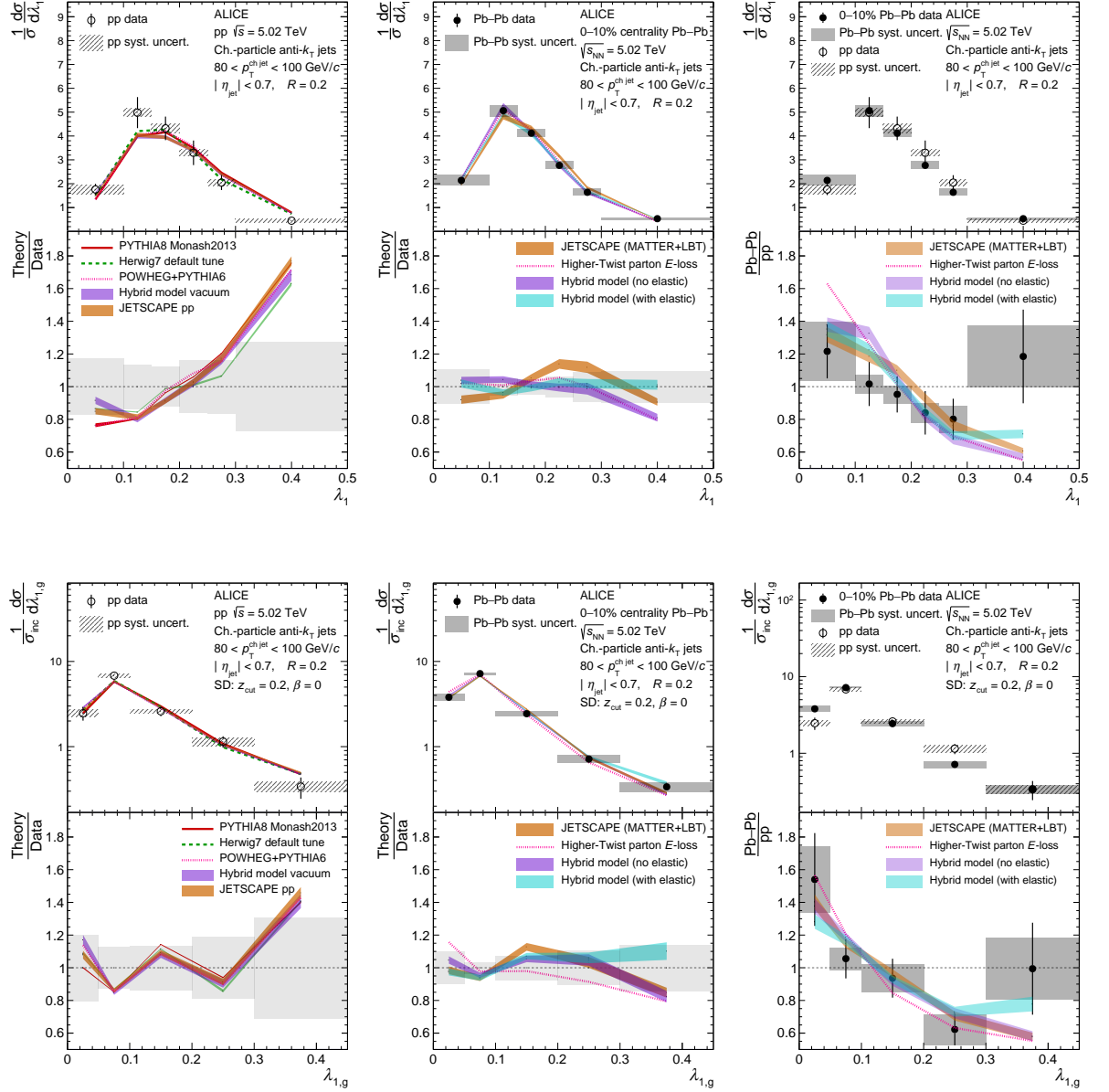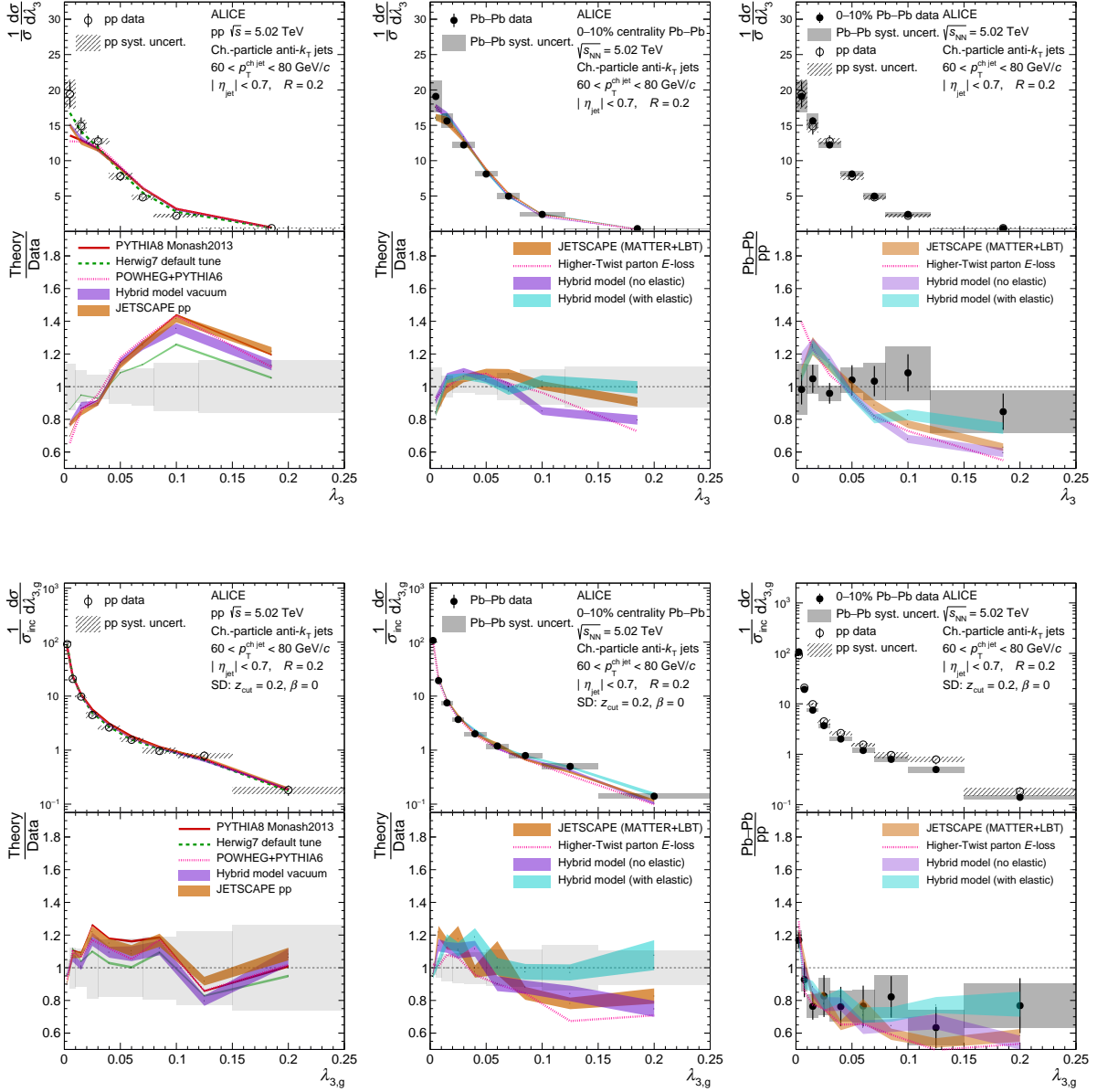
**Fig. 4:** ALICE measurement of ungroomed (top) and SD groomed (bottom) $\lambda_1$ for $R = 0.2$ charged-particle jets in pp (left) and Pb–Pb (middle) collisions at $\sqrt{s_{\text{NN}}} = 5.02$ TeV for $80 < p_{\text{T}}^{\text{ch jet}} < 100$ GeV/$c$ as compared to models. The ratio of Pb–Pb to pp is also shown (right), which quantifies the substructure modifications from quenching. The pp result is taken from Ref. [35].
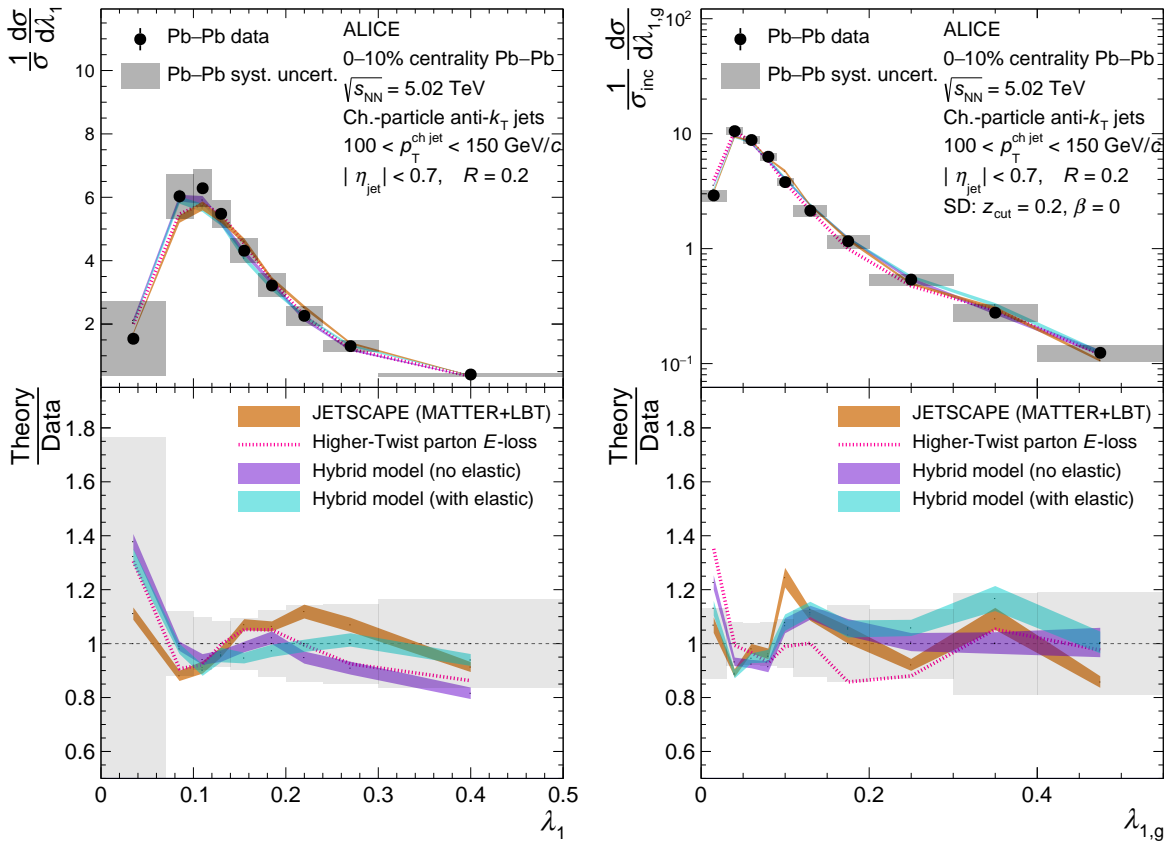
**Fig. 5:** ALICE measurement of ungroomed (left) and SD groomed (right) $\lambda_1$ for $R = 0.2$ charged-particle jets in Pb–Pb collisions at $\sqrt{s_{NN}} = 5.02$ TeV for $100 < p_T^{\text{ch jet}} < 150$ GeV/$c$ as compared to models.
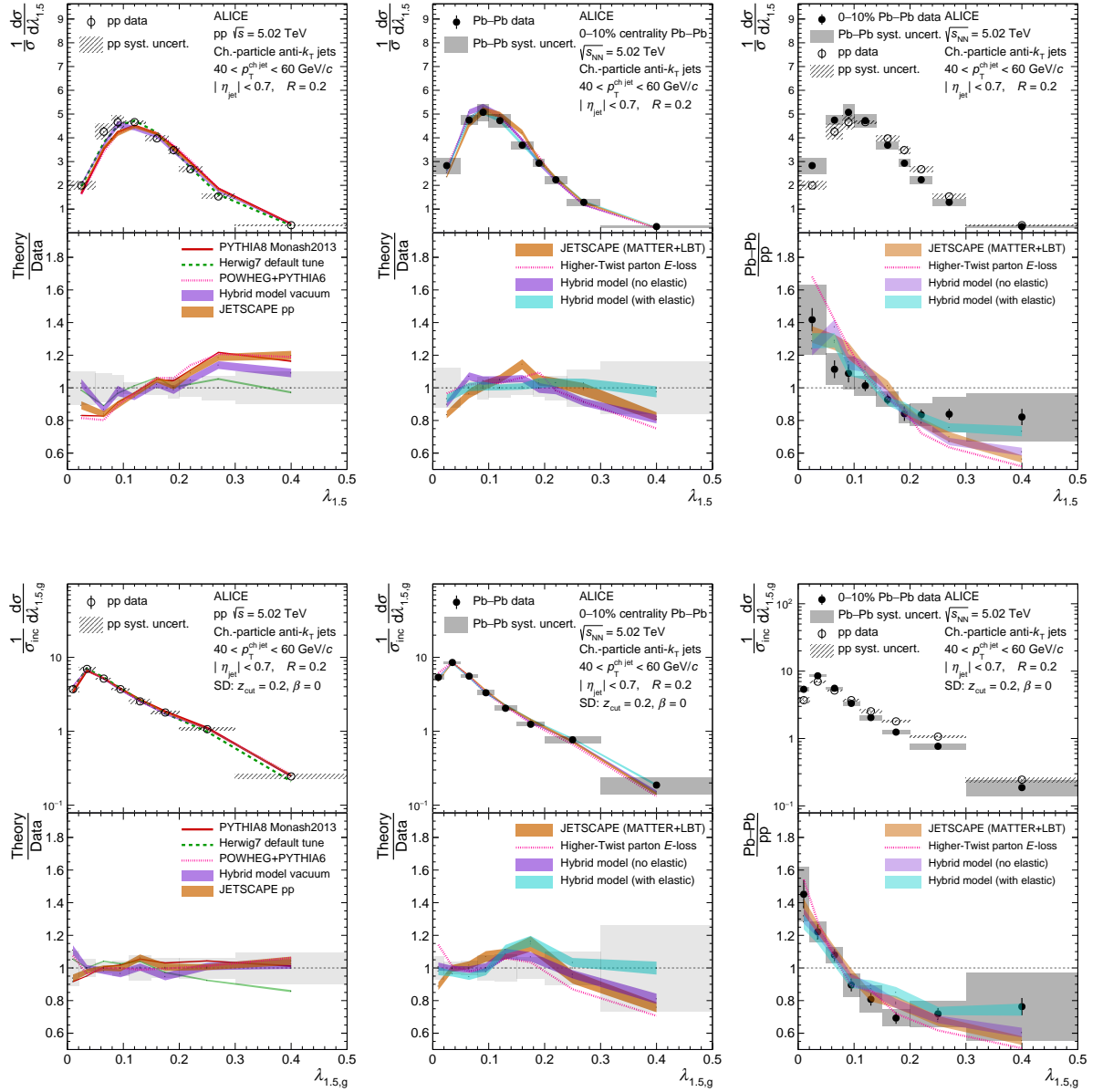
**Fig. 6:** ALICE measurement of ungroomed (top) and SD groomed (bottom) $\lambda_{1.5}$ for $R = 0.2$ charged-particle jets in pp (left) and Pb–Pb (middle) collisions at $\sqrt{s_{\mathrm{NN}}} = 5.02$ TeV for $40 < p_{\mathrm{T}}^{\mathrm{ch\,jet}} < 60$ GeV/$c$ as compared to models. The ratio of Pb–Pb to pp is also shown (right), which quantifies the substructure modifications from quenching. The pp result is taken from Ref. [35].
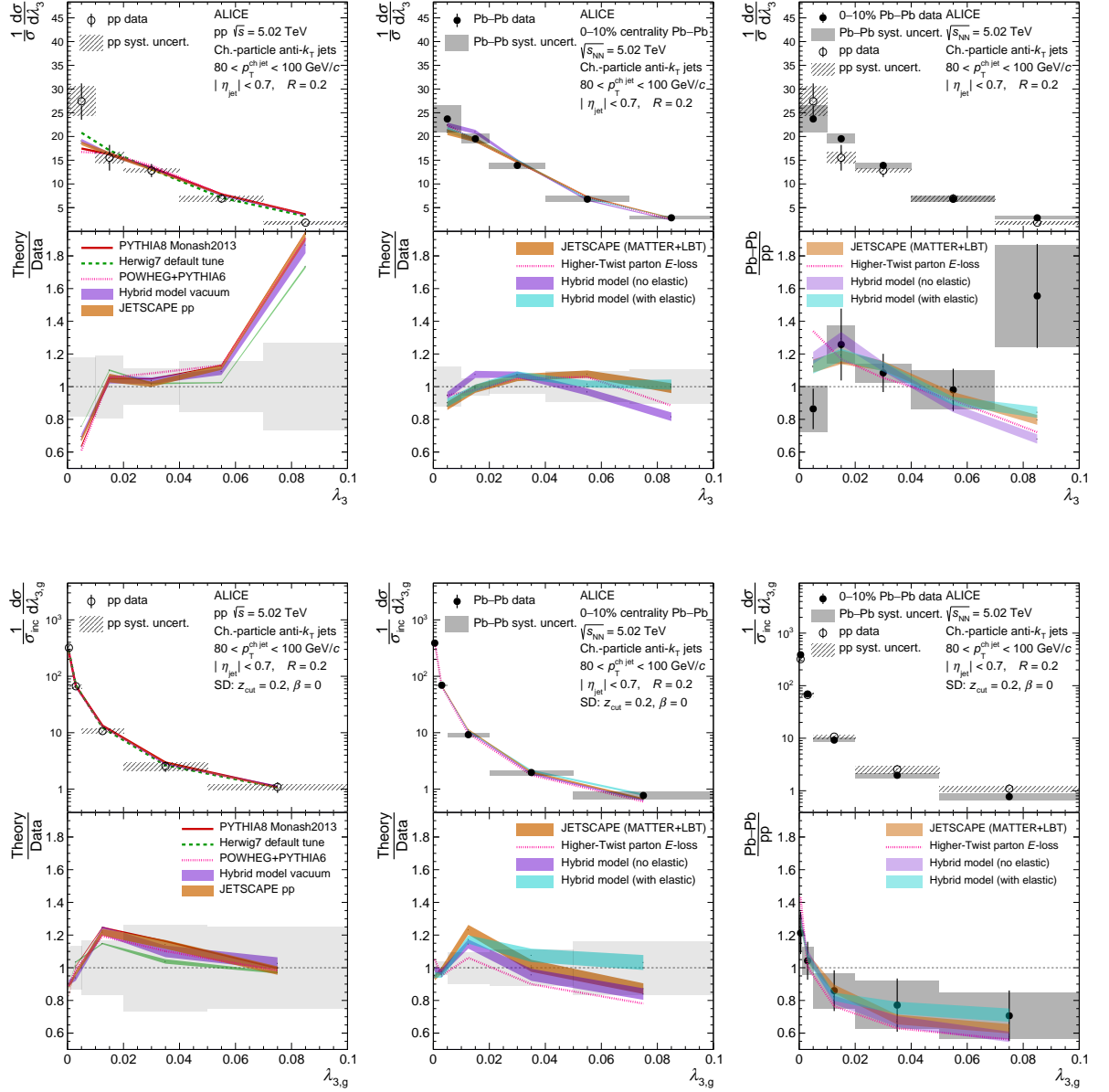
**Fig. 7:** ALICE measurement of ungroomed (top) and SD groomed (bottom) $\lambda_{1.5}$ for $R = 0.2$ charged-particle jets in pp (left) and Pb–Pb (middle) collisions at $\sqrt{s_{NN}} = 5.02$ TeV for $60 < p_T^{ch\,jet} < 80$ GeV/$c$ as compared to models. The ratio of Pb–Pb to pp is also shown (right), which quantifies the substructure modifications from quenching. The pp result is taken from Ref. [35].
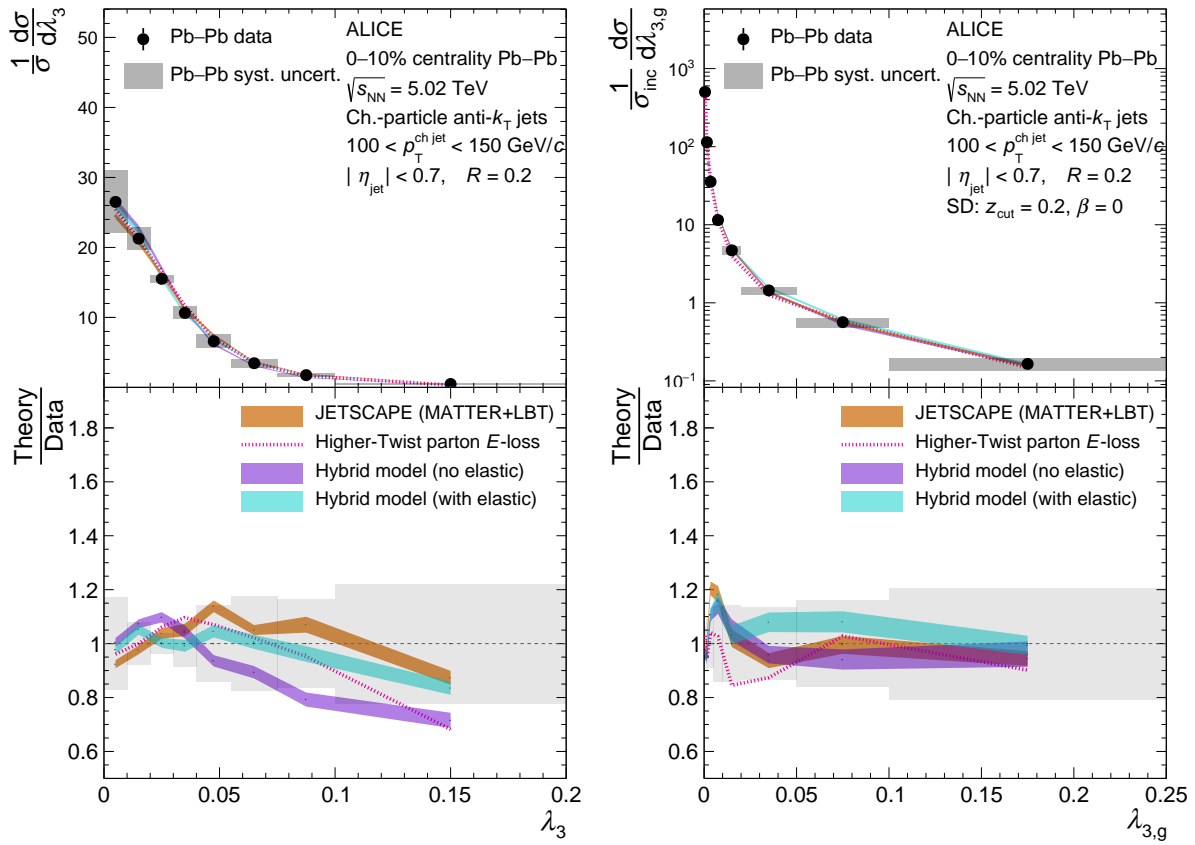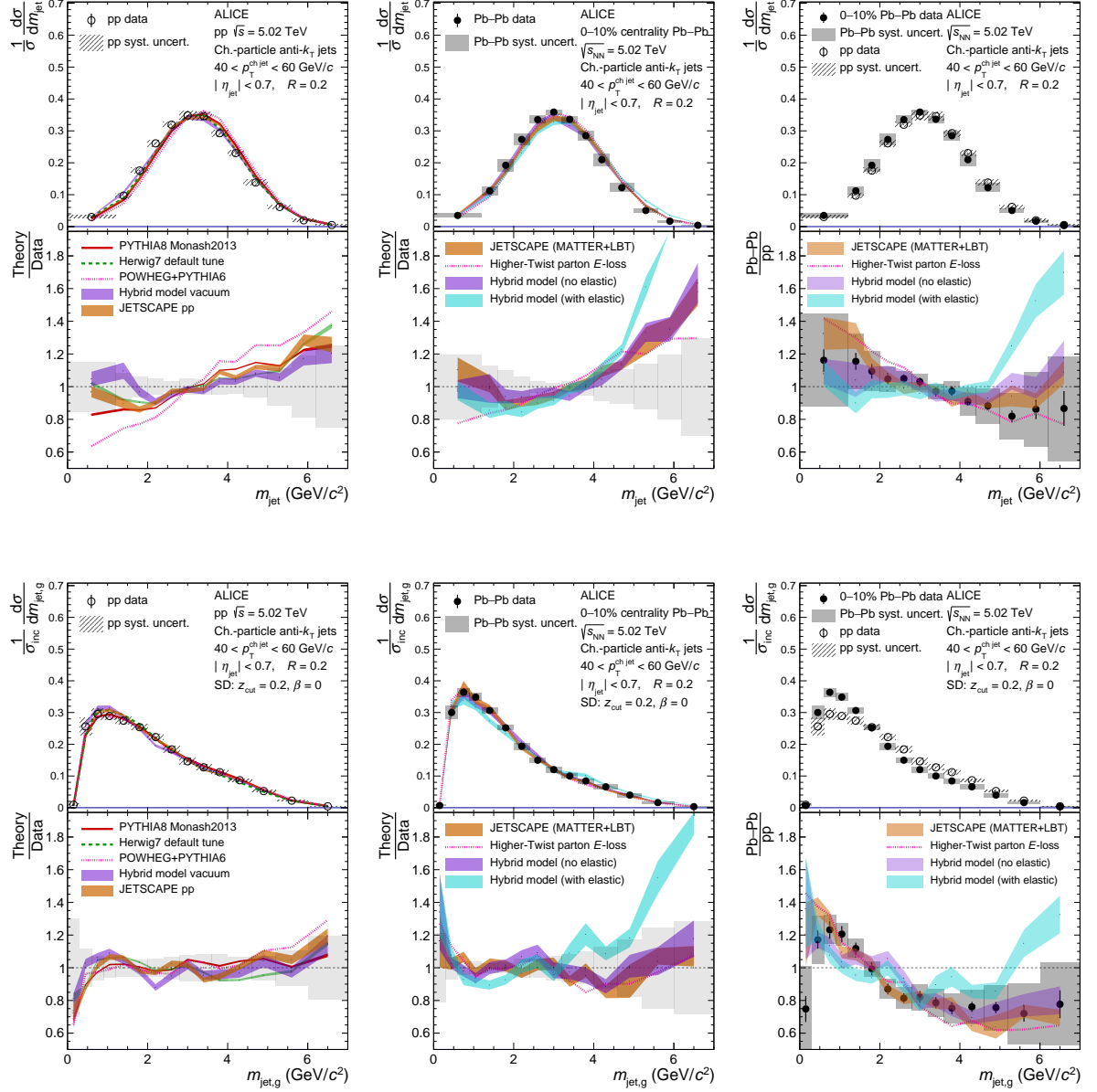
**Fig. 8:** ALICE measurement of ungroomed (top) and SD groomed (bottom) $\lambda_{1.5}$ for $R = 0.2$ charged-particle jets in pp (left) and Pb–Pb (middle) collisions at $\sqrt{s_{NN}} = 5.02$ TeV for $80 < p_T^{ch\,jet} < 100$ GeV/$c$ as compared to models. The ratio of Pb–Pb to pp is also shown (right), which quantifies the substructure modifications from quenching. The pp result is taken from Ref. [35].

**Fig. 9:** ALICE measurement of ungroomed (left) and SD groomed (right) $\lambda_{1.5}$ for $R = 0.2$ charged-particle jets in Pb–Pb collisions at $\sqrt{s_{\mathrm{NN}}} = 5.02$ TeV for $100 < p_{\mathrm{T}}^{\mathrm{ch\,jet}} < 150$ GeV/$c$ as compared to models.

**Fig. 10:** ALICE measurement of ungroomed (top) and SD groomed (bottom) $\lambda_2$ for $R = 0.2$ charged-particle jets in pp (left) and Pb–Pb (middle) collisions at $\sqrt{s_{\rm NN}} = 5.02$ TeV for $40 < p_{\rm T}^{\rm ch\,jet} < 60$ GeV/$c$ as compared to models. The ratio of Pb–Pb to pp is also shown (right), which quantifies the substructure modifications from quenching. The pp result is taken from Ref. [35], while the rightmost panels are similarly reported in Ref. [36].
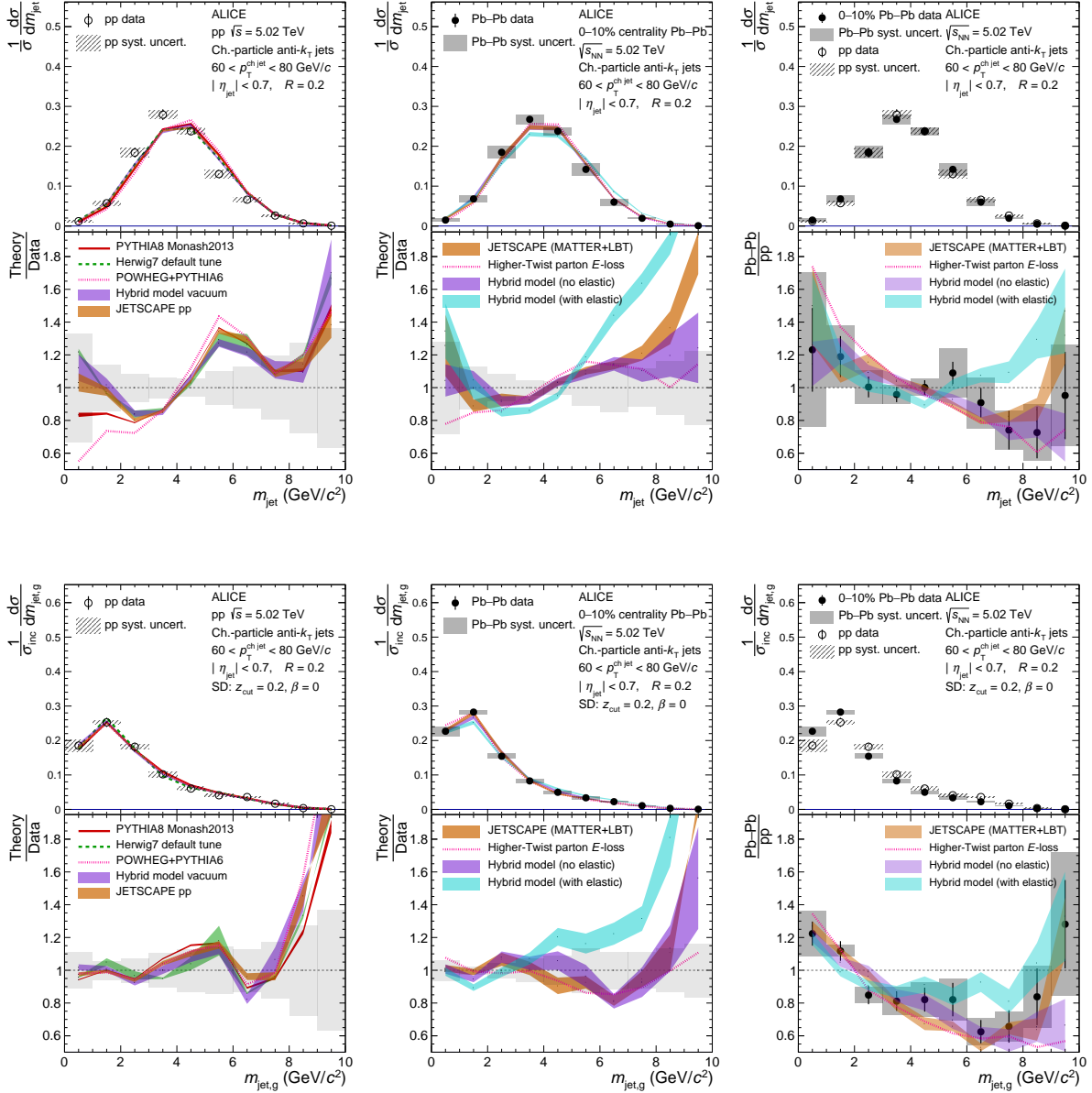
**Fig. 11:** ALICE measurement of ungroomed (top) and SD groomed (bottom) $\lambda_2$ for $R = 0.2$ charged-particle jets in pp (left) and Pb–Pb (middle) collisions at $\sqrt{s_{\mathrm{NN}}} = 5.02$ TeV for $60 < p_{\mathrm{T}}^{\mathrm{ch\,jet}} < 80$ GeV/$c$ as compared to models. The ratio of Pb–Pb to pp is also shown (right), which quantifies the substructure modifications from quenching. The pp result is taken from Ref. [35].
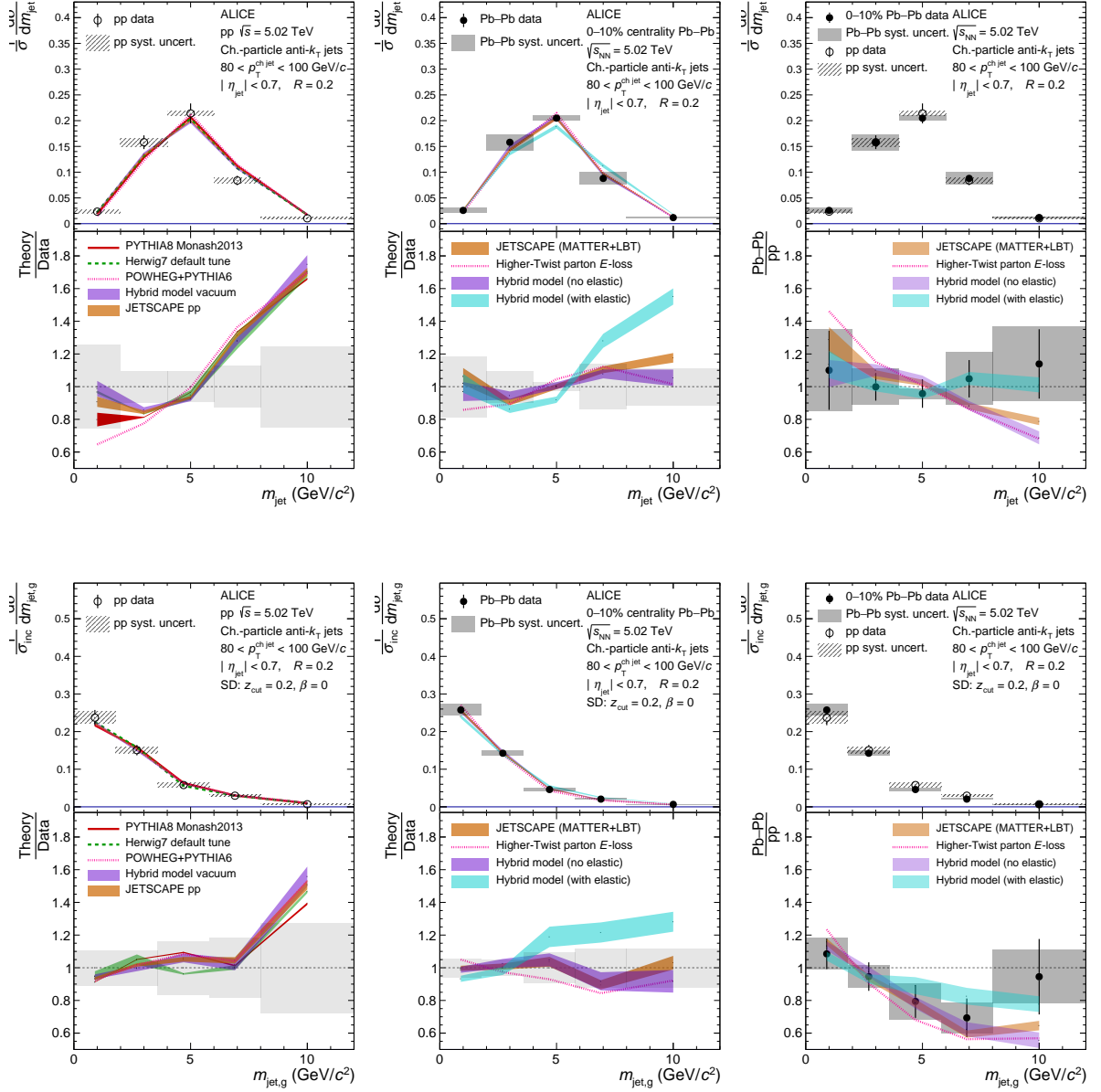
**Fig. 12:** ALICE measurement of ungroomed (top) and SD groomed (bottom) $\lambda_2$ for $R = 0.2$ charged-particle jets in pp (left) and Pb–Pb (middle) collisions at $\sqrt{s_{NN}} = 5.02$ TeV for $80 < p_T^{ch\,jet} < 100$ GeV/$c$ as compared to models. The ratio of Pb–Pb to pp is also shown (right), which quantifies the substructure modifications from quenching. The pp result is taken from Ref. [35].
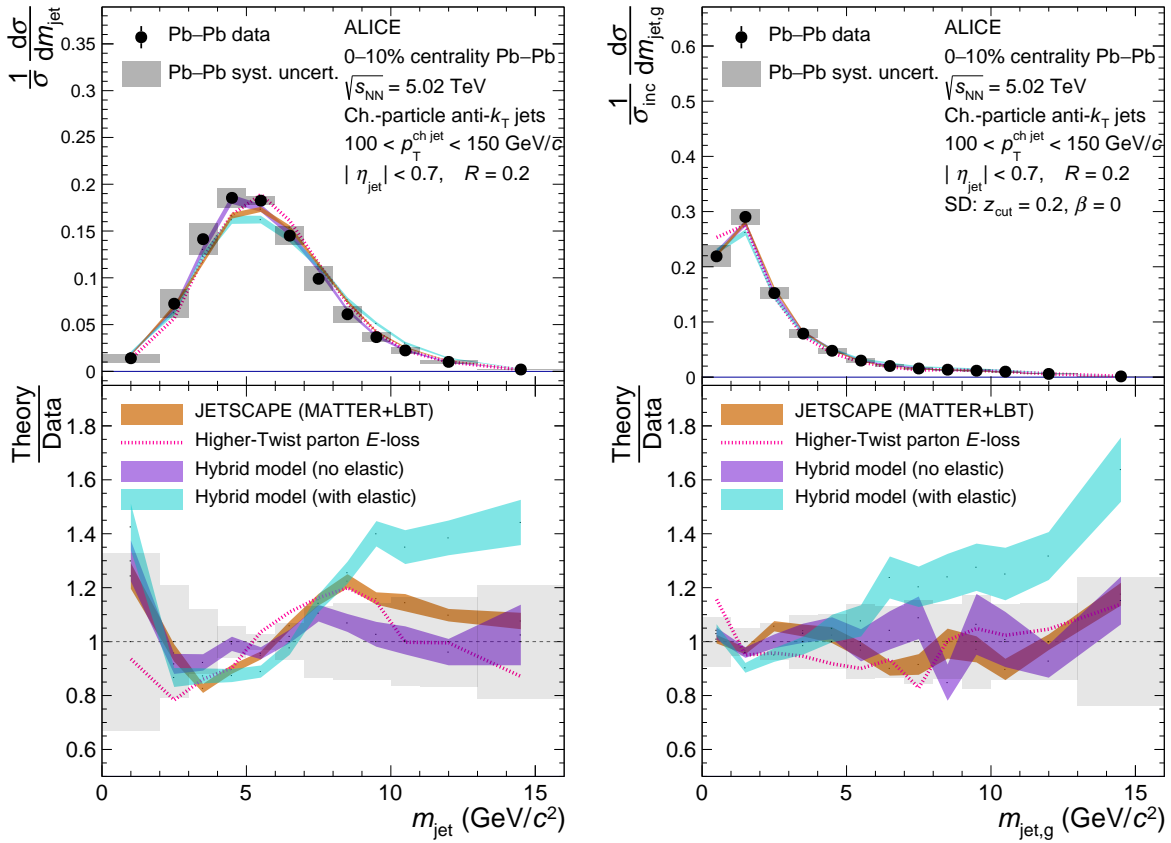
**Fig. 13:** ALICE measurement of ungroomed (left) and SD groomed (right) $\lambda_2$ for $R = 0.2$ charged-particle jets in Pb–Pb collisions at $\sqrt{s_{NN}} = 5.02$ TeV for $100 < p_T^{ch\,jet} < 150$ GeV/$c$ as compared to models.

**Fig. 14:** ALICE measurement of ungroomed (top) and SD groomed (bottom) $\lambda_3$ for $R = 0.2$ charged-particle jets in pp (left) and Pb–Pb (middle) collisions at $\sqrt{s_{\text{NN}}} = 5.02$ TeV for $40 < p_{\text{T}}^{\text{ch jet}} < 60$ GeV/$c$ as compared to models. The ratio of Pb–Pb to pp is also shown (right), which quantifies the substructure modifications from quenching. The pp result is taken from Ref. [35], while the rightmost panels are similarly reported in Ref. [36].

**Fig. 15:** ALICE measurement of ungroomed (top) and SD groomed (bottom) $\lambda_3$ for $R = 0.2$ charged-particle jets in pp (left) and Pb–Pb (middle) collisions at $\sqrt{s_{\mathrm{NN}}} = 5.02$ TeV for $60 < p_{\mathrm{T}}^{\mathrm{ch\ jet}} < 80$ GeV/$c$ as compared to models. The ratio of Pb–Pb to pp is also shown (right), which quantifies the substructure modifications from quenching. The pp result is taken from Ref. [35]

**Fig. 16:** ALICE measurement of ungroomed (top) and SD groomed (bottom) $\lambda_3$ for $R = 0.2$ charged-particle jets in pp (left) and Pb–Pb (middle) collisions at $\sqrt{s_{\text{NN}}} = 5.02$ TeV for $80 < p_{\text{T}}^{\text{ch jet}} < 100$ GeV/$c$ as compared to models. The ratio of Pb–Pb to pp is also shown (right), which quantifies the substructure modifications from quenching. The pp result is taken from Ref. [35]

**Fig. 17:** ALICE measurement of ungroomed (left) and SD groomed (right) $\lambda_3$ for $R = 0.2$ charged-particle jets in Pb–Pb collisions at $\sqrt{s_{\mathrm{NN}}} = 5.02$ TeV for $100 < p_{\mathrm{T}}^{\mathrm{ch\,jet}} < 150$ GeV/$c$ as compared to models.

**Fig. 18:** ALICE measurement of ungroomed (top) and SD groomed (bottom) $m_{\rm jet}$ for $R = 0.2$ charged-particle jets in pp (left) and Pb–Pb (middle) collisions at $\sqrt{s_{\rm NN}} = 5.02$ TeV for $40 < p_{\rm T}^{\rm ch\ jet} < 60$ GeV/$c$ as compared to models. The ratio of Pb–Pb to pp is also shown (right), which quantifies the substructure modifications from quenching. The pp result is taken from Ref. [35], while the rightmost panels are similarly reported in Ref. [36].

**Fig. 19:** ALICE measurement of ungroomed (top) and SD groomed (bottom) $m_{jet}$ for $R = 0.2$ charged-particle jets in pp (left) and Pb–Pb (middle) collisions at $\sqrt{s_{NN}} = 5.02$ TeV for $60 < p_T^{ch\,jet} < 80$ GeV/$c$ as compared to models. The ratio of Pb–Pb to pp is also shown (right), which quantifies the substructure modifications from quenching. The pp result is taken from Ref. [35]

**Fig. 20:** ALICE measurement of ungroomed (top) and SD groomed (bottom) $m_{jet}$ for $R = 0.2$ charged-particle jets in pp (left) and Pb–Pb (middle) collisions at $\sqrt{s_{NN}} = 5.02$ TeV for $80 < p_T^{ch\,jet} < 100$ GeV/$c$ as compared to models. The ratio of Pb–Pb to pp is also shown (right), which quantifies the substructure modifications from quenching. The pp result is taken from Ref. [35]

**Fig. 21:** ALICE measurement of ungroomed (left) and SD groomed (right) $m_{jet}$ for $R = 0.2$ charged-particle jets in Pb–Pb collisions at $\sqrt{s_{NN}} = 5.02$ TeV for $100 < p_T^{ch\,jet} < 150$ GeV/$c$ as compared to models.

## 5.1    Comparing Pb–Pb and pp collisions

In high-energy heavy-ion collisions, the internal structure of jets undergo modifications via scatterings of jet fragments with the hot and dense QCD medium. Measurements of the groomed and ungroomed $\lambda_\alpha$ and $m_{\text{jet}}$, reported above, probe the angular dependence of jet quenching and seek to clarify previous measurements where a vacuum baseline was unavailable.

In comparing the Pb–Pb and pp distributions, a significant "narrowing" effect in Pb–Pb collisions with respect to pp collisions is observed via an enhancement at small values of angularity (mass), and a corresponding suppression at large values. For the jet angularities, the narrowing is strongest at low $\alpha$ and decreases at larger values of $\alpha$, since larger values of $\alpha$ increase the weighting of large-angle radiations, corresponding to a strongly quenched jet core. This conclusion is supported by a significant enhancement in the narrowing for SD groomed jets, which remove soft radiation at wide angles, as compared to ungroomed jets. The narrowing is also observed in the jet mass distributions, where jets with intermediate-to high-$m_{\text{jet}}$ are suppressed in Pb–Pb as compared to pp. Some distributions, however, show hints of a possible enhancement at very large $m_{\text{jet}}$, which might be expected from sequential in-medium hard scatterings, though the ratios are consistent with unity (i.e. no modification) within experimental uncertainties. The strength of quenching appears to be consistent across the reported $p_{\text{T}}^{\text{ch jet}}$ range within the reported uncertainties, though the behavior is most obvious at low-$p_{\text{T}}^{\text{ch jet}}$ where statistical uncertainties are the smallest.

Earlier LHC Run 1 comparisons of Pb–Pb data to vacuum MC simulations generated with PYTHIA8 show even stronger modification, with both tails of the distribution modified by an approximate factor of 2 [34]. However, these new Run 2 results are compared to baselines from pp data taken at equivalent center-of-mass energy, which comparatively reduces this narrowing effect. A proper pp baseline is therefore essential for correctly interpreting measurements of jet quenching in an unbiased way. This conclusion has far-reaching implications for future runs at the LHC: heavy-ion data must pair with statistically consistent jet samples in pp, where smaller collision systems result in fewer jets.

## 5.2    Comparison to theoretical models

We compare the ratio of the measurements in pp and Pb–Pb collisions to several theoretical implementations of jet quenching.

**JETSCAPE.** The predictions by the JETSCAPE Collaboration [65] are extracted from a Monte Carlo implementation of multi-stage energy loss with the MATTER [66] medium-modified parton shower model controlling the high-virtuality phase and the Linear Boltzmann Transport (LBT) model [67] describing the low-virtuality phase. The version of JETSCAPE used for this calculation employs a jet transport coefficient, $\hat{q}$, that includes dependence on parton virtuality, in addition to dependence on the local temperature and running of the parton-medium coupling. The JETSCAPE predictions reproduce the measurements well.

**Higher-Twist parton energy loss.** The predictions by Yan et al. [68] use POWHEG matching of NLO matrix elements to the PYTHIA parton shower [69] as a baseline and apply the Higher-Twist formalism for jet–medium interactions. The initial position in the QGP of the produced partons is sampled from a Glauber model [70], and as the parton propagates, it emits medium-induced gluon radiation based on the $\hat{q}$-dependent Higher-Twist approach [71–74], with the smooth iEBE-VISHNU hydro model [75] providing the evolution profile of the QGP medium. These predictions describe the $\lambda_\alpha$ and $m_{\text{jet}}$ measurements well.

**Hybrid model.** The predictions by Pablos et al. [76], known as the Hybrid model, consist of partons produced by a vacuum shower that interact with the medium according to a strongly-coupled AdS/CFT-based model. Hybrid model predictions are generated with a wake behind the jet, created by the partonic

energy lost due to medium-induced emissions [77]. These predictions are produced both with and without elastic Molière scattering of medium scattering centers [78], which are hypothesized to arise from the particle nature of the fluid at high energies, or from possible emergent structures.

The $m_{\text{jet}}$ data strongly favor the Hybrid model predictions without Molière scattering, supporting a picture where the dominant energy loss mechanism in these systems is gluon-induced radiation. The $\lambda_\alpha$ data are less discriminating on Molière effects, with both predictions describing the data within experimental uncertainties; however, the with-elastic case tends to be closer to the central values of the data points than the no-elastic case. This presents an opportunity to reevaluate the strength of Molière effects and how their behavior should affect different observables.

Despite employing different microscopic implementations of the jet-medium interactions, the majority of the models capture the qualitative feature of the narrowing seen in the ratio of $\lambda_\alpha$ and $m_{\text{jet}}$ distributions in Pb–Pb versus pp. The Higher-Twist model predictions tend to predict the strongest narrowing behavior, while JETSCAPE produces predictions which are very similar to the Hybrid model without Molière effects. Slight tension is observed between the data and models in the higher $p_{\text{T}}^{\text{ch jet}}$ bins, though the predictions are still generally within the large statistical and systematic uncertainties. Models tend to perform better for the groomed observables than for the ungroomed ones, as grooming removes nonperturbative, soft gluon radiations which are more difficult to model theoretically than the hard parton which initiates the jet. These comparisons provide new insight to the nature of these modifications, and as outlined in the following section, indicate promising directions for further studies.

## 5.3 Discussion

In order to study the girth–mass inconsistency in light of Eq. 3, ALICE has performed new measurements of $m_{\text{jet}}$ and $\lambda_2^1$ using the same jet sample for the first time. While Eq. 3 relates $m_{\text{jet}}$ and $\lambda_2$ directly to one another, model comparisons show differing behavior. The Hybrid model with elastic Molière scattering, for example, vastly overestimates the data at large values of $m_{\text{jet}}$, while it agrees with or even slightly underestimates the yield at large $\lambda_2$. Since the distributions are positive definite and obey square proportionality following Eq. 3, large corrections to Eq. 3 must apply at these values of $p_{\text{T}}^{\text{ch jet}}$. These could include nonperturbative effects such as hadronization or higher-order correction terms $\mathcal{O}[(\lambda_2)^2]$. Despite their mathematical similarity, underlying physical differences between the two observables exist: the jet mass is sensitive to quark masses, whereas the IRC-safe jet angularities are sensitive to fragmentation and quark- versus gluon-initiated jet differences. Identifying the variations in the measured distributions as these physical differences of the observables explains the girth–mass difference.

This observation highlights the importance of making broad measurements of quenched jet substructure, as closely-related observables can provide significantly different probes of underlying physical phenomena. Studies of quenched jets using $N$-subjettiness variables as a basis suggest that dozens of such observables may be required to optimally characterize quenched jet behavior [79].

These measurements are not able to significantly differentiate between JETSCAPE, the Higher-Twist formalism, and the Hybrid model without elastic scattering. The addition of elastic Molière scattering to the Hybrid approach enhances wide-angle constituents and correspondingly boosts the quenching modification at large $m_{\text{jet}}$ and $\lambda_\alpha$; however, this effect greatly reduces agreement with experimental data for $m_{\text{jet}}$. The jet narrowing observed in Pb–Pb data as compared to pp is strongest at smaller values of $\alpha$ and with soft drop grooming, revealing a strongly-quenched jet core.

As discussed above, jet grooming enhances the perturbative calculability of jet substructure observables, while its use in heavy-ion collisions additionally reduces contamination from the thermal background. Compared to their ungroomed counterparts, the groomed $\lambda_\alpha$ and $m_{\text{jet}}$ distributions display reduced systematic uncertainties and an enhanced narrowing effect, consistent with a strongly quenched jet core. Increased similarity between models also suggests perturbative agreement and a continuing need for prob-

ing nonperturbative effects. For the jet angularities, several model predictions converge with grooming, limiting the differentiating power between them – despite different theoretical approaches. Scrutinizing jet quenching models therefore requires consideration of both the significant nonperturbative and perturbative effects.

## 6 Conclusion

We provide measurements of jet angularities, mass, and their medium-induced modifications in Pb–Pb collisions both with and without grooming. These results depict a consistent picture of narrowing as jets traverse the QGP, which is dominated by a collinearized jet core. By measuring both $m_{\mathrm{jet}}$ and jet thrust ($\lambda_2$) using the same jets, and by also measuring the appropriate pp baseline, we reexamine the girth–mass inconsistency raised by earlier measurements, which showed conflicting quenching behavior in these related observables. We again observe fundamental differences between these observables and deduce that the mass–thrust relation (Eq. 3) must depend on significant higher-order corrections or on nonperturbative physics at these low $p_{\mathrm{T}}^{\mathrm{ch\,jet}}$, where the strong coupling $\alpha_S$ is large.

The data generally agree with models including in-medium energy loss. The jet mass prefers no in-medium elastic Molière scattering (within the Hybrid model), but the jet angularities slightly prefer if this process is included. Theory comparisons also reveal that a pp baseline is essential for evaluating quenching behavior of jet substructure and should always be measured to fully profit from heavy-ion runs at the LHC. Compared to previous measurements using a MC simulated pp baseline, quenching effects of these results are reduced.

While jet grooming has been used in many recent measurements, the phase space of groomed observables remains mostly unexplored. Using grooming to reduce experimental uncertainties while selecting observables which probe effects such as in-medium color coherence will be essential to illuminate medium structure and the origins of jet quenching. Grooming can also be used to reduce nonperturbative effects, providing a handle between groomed and ungroomed observables to isolate these mechanisms in the QGP.

# References

[1] J. D. Bjorken, "Highly relativistic nucleus-nucleus collisions: The central rapidity region", *Phys. Rev. D* **27** (1983) 140–151.

[2] W. Busza, K. Rajagopal, and W. van der Schee, "Heavy Ion Collisions: The Big Picture, and the Big Questions", *Ann. Rev. Nucl. Part. Sci.* **68** (2018) 339–376, `arXiv:1802.04801 [hep-ph]`.

[3] J. D. Bjorken, "Energy Loss of Energetic Partons in Quark-Gluon Plasma: Possible Extinction of High $p_T$ jets in Hadron-Hadron Collisions." Fermilab, 1982.
`https://lss.fnal.gov/archive/preprint/fermilab-pub-82-059-t.shtml`.

[4] D. A. Appel, "Jets as a probe of quark-gluon plasmas", *Phys. Rev. D* **33** (1986) 717–722.

[5] M. Gyulassy and M. Plümer, "Jet Quenching in Dense Matter", *Phys. Lett. B* **243** (1990) 432–438.

[6] R. Baier, Y. Dokshitzer, S. Peigné, and D. Schiff, "Induced gluon radiation in a QCD medium", *Phys. Lett. B* **345** (1995) 277–286, `arXiv:hep-ph/9411409`.

[7] S. Cao and X.-N. Wang, "Jet quenching and medium response in high-energy heavy-ion collisions: a review", *Rep. Prog. Phys.* **84** (2021) 024301.

[8] Y. Mehtar-Tani and K. Tywoniuk, "Groomed jets in heavy-ion collisions: sensitivity to medium-induced bremsstrahlung", *JHEP* **4** (2017) 125, `arXiv:1610.08930 [hep-ph]`.

[9] Y.-T. Chien and R. Kunnawalkam Elayavalli, "Probing heavy ion collisions using quark and gluon jet substructure", `arXiv:1803.03589 [hep-ph]`.

[10] **CMS** Collaboration, S. Chatrchyan *et al.*, "Studies of jet mass in dijet and W/Z + jet events", *JHEP* **5** (2013) 090, `arXiv:1303.4811 [hep-ex]`.

[11] **ALICE** Collaboration, S. Acharya *et al.*, "First measurement of jet mass in Pb–Pb and p–Pb collisions at the LHC", *Phys. Lett. B* **776** (2018) 249–264, `arXiv:1702.00804 [nucl-ex]`.

[12] **CMS** Collaboration, A. M. Sirunyan *et al.*, "Measurement of the jet mass in highly boosted $t\bar{t}$ events from pp collisions at $\sqrt{s} = 8$ TeV", *Eur. Phys. J. C* **77** (2017) 467, `arXiv:1703.06330 [hep-ex]`.

[13] **ATLAS** Collaboration, M. Aaboud *et al.*, "A measurement of the soft-drop jet mass in pp collisions at $\sqrt{s} = 13$ TeV with the ATLAS detector", *Phys. Rev. Lett.* **121** (2018) 092001, `arXiv:1711.08341 [hep-ex]`.

[14] **CMS** Collaboration, A. M. Sirunyan *et al.*, "Measurement of the groomed jet mass in PbPb and pp collisions at $\sqrt{s_{\mathrm{NN}}} = 5.02$ TeV", *JHEP* **10** (2018) 161, `arXiv:1805.05145 [hep-ex]`.

[15] **CMS** Collaboration, A. M. Sirunyan *et al.*, "Measurements of the differential jet cross section as a function of the jet mass in dijet events from proton-proton collisions at $\sqrt{s} = 13$ TeV", *JHEP* **11** (2018) 113, `arXiv:1807.05974 [hep-ex]`.

[16] **ATLAS** Collaboration, M. Aaboud *et al.*, "Properties of $g \rightarrow b\bar{b}$ at small opening angles in $pp$ collisions with the ATLAS detector at $\sqrt{s} = 13$ TeV", *Phys. Rev. D* **99** (2019) 052004, `arXiv:1812.09283 [hep-ex]`.

[17] **ATLAS** Collaboration, G. Aad *et al.*, "A measurement of soft-drop jet observables in $pp$ collisions with the ATLAS detector at $\sqrt{s} = 13$ TeV", *Phys. Rev. D* **101** (2020) 052007, `arXiv:1912.09837 [hep-ex]`.

[18] **ATLAS** Collaboration, G. Aad *et al.*, "Measurement of the jet mass in high transverse momentum $Z(\rightarrow b\bar{b})\gamma$ production at $\sqrt{s} = 13$ TeV using the ATLAS detector", *Phys. Lett. B* **812** (2021) 135991, `arXiv:1907.07093 [hep-ex]`.

[19] **CMS** Collaboration, A. M. Sirunyan *et al.*, "Measurement of the jet mass distribution and top quark mass in hadronic decays of boosted top quarks in pp collisions at $\sqrt{s} = 13$ TeV", *Phys. Rev. Lett.* **124** (2020) 202001, `arXiv:1911.03800 [hep-ex]`.

[20] **CMS** Collaboration, A. Tumasyan *et al.*, "Measurement of the jet mass distribution and top quark mass in hadronic decays of boosted top quarks in proton-proton collisions at $\sqrt{s} = 13$ TeV", `arXiv:2211.01456 [hep-ex]`.

[21] M. Dasgupta, A. Fregoso, S. Marzani, and G. P. Salam, "Towards an understanding of jet substructure", *JHEP* **09** (2013) 029, arXiv:1307.0007 [hep-ph].

[22] S. Marzani, L. Schunk, and G. Soyez, "A study of jet mass distributions with grooming", *JHEP* **07** (2017) 132, arXiv:1704.02210 [hep-ph].

[23] S. Marzani, L. Schunk, and G. Soyez, "The jet mass distribution after Soft Drop", *Eur. Phys. J. C* **78** (2018) 96, arXiv:1712.05105 [hep-ph].

[24] A. Kardos, A. J. Larkoski, and Z. Trócsányi, "Groomed jet mass at high precision", *Phys. Lett. B* **809** (2020) 135704, arXiv:2002.00942 [hep-ph].

[25] C. F. Berger, T. Kúcs, and G. F. Sterman, "Interjet energy flow/event shape correlations", *Int. J. Mod. Phys. A* **18** (2003) 4159–4168, arXiv:hep-ph/0212343.

[26] C. F. Berger, T. Kúcs, and G. F. Sterman, "Event shape/energy flow correlations", *Phys. Rev. D* **68** (2003) 014012, arXiv:hep-ph/0303051.

[27] C. F. Berger and L. Magnea, "Scaling of power corrections for angularities from dressed gluon exponentiation", *Phys. Rev. D* **70** (2004) 094010, arXiv:hep-ph/0407024.

[28] L. G. Almeida, S. J. Lee, G. Perez, G. F. Sterman, I. Sung, and J. Virzi, "Substructure of high-$p_\mathrm{T}$ jets at the LHC", *Phys. Rev. D* **79** (2009) 074017, arXiv:0807.0234 [hep-ph].

[29] A. J. Larkoski, J. Thaler, and W. J. Waalewijn, "Gaining (mutual) information about quark/gluon discrimination", *JHEP* **11** (2014) 129, arXiv:1408.3122 [hep-ph].

[30] C. F. Berger and G. F. Sterman, "Scaling rule for nonperturbative radiation in a class of event shapes", *JHEP* **09** (2003) 058, arXiv:hep-ph/0307394.

[31] E. Farhi, "Quantum Chromodynamics Test for Jets", *Phys. Rev. Lett.* **39** (1977) 1587–1588.

[32] Z.-B. Kang, K. Lee, and F. Ringer, "Jet angularity measurements for single inclusive jet production", *JHEP* **04** (2018) 110, arXiv:1801.00790 [hep-ph].

[33] S. Catani, G. Turnock, and B. Webber, "Jet broadening measures in $e^+e^-$ annihilation", *Phys. Lett. B* **295** (1992) 269–276.

[34] **ALICE** Collaboration, S. Acharya *et al.*, "Medium modification of the shape of small-radius jets in central Pb-Pb collisions at $\sqrt{s_\mathrm{NN}} = 2.76$ TeV", *JHEP* **10** (2018) 139, arXiv:1807.06854 [nucl-ex].

[35] **ALICE** Collaboration, S. Acharya *et al.*, "Measurements of the groomed and ungroomed jet angularities in pp collisions at $\sqrt{s} = 5.02$ TeV", *JHEP* **05** (2022) 061, arXiv:2107.11303 [nucl-ex].

[36] **ALICE** Collaboration, S. Acharya *et al.*, "Medium-induced modification of the groomed and ungroomed jet mass and angularities in Pb–Pb collisions at $\sqrt{s_\mathrm{NN}} = 5.02$ TeV", 2024.

[37] A. J. Larkoski, S. Marzani, G. Soyez, and J. Thaler, "Soft Drop", *JHEP* **05** (2014) 146, arXiv:1402.2657 [hep-ph].

[38] **ALICE** Collaboration, K. Aamodt *et al.*, "The ALICE experiment at the CERN LHC", *JINST* **3** (2008) S08002.

[39] **ALICE** Collaboration, B. B. Abelev *et al.*, "Performance of the ALICE Experiment at the CERN LHC", *Int. J. Mod. Phys. A* **29** (2014) 1430044, arXiv:1402.4476 [nucl-ex].

[40] **ALICE** Collaboration, E. Abbas *et al.*, "Performance of the ALICE VZERO system", *JINST* **8** (2013) P10016, `arXiv:1306.3130 [nucl-ex]`.

[41] **ALICE** Collaboration, B. Abelev *et al.*, "Centrality determination of Pb–Pb collisions at $\sqrt{s} = 2.76$ TeV with ALICE", *Phys. Rev. C* **88** (2013) 044909, `arXiv:1301.4361 [nucl-ex]`.

[42] **ALICE** Collaboration, S. Acharya *et al.*, "Centrality determination in heavy-ion collisions." `http://cds.cern.ch/record/2636623`.

[43] **ALICE** Collaboration, S. Acharya *et al.*, "ALICE 2017 luminosity determination for pp collisions at $\sqrt{s} = 5$ TeV",. `http://cds.cern.ch/record/2648933`.

[44] **ALICE** Collaboration, S. Acharya *et al.*, "ALICE luminosity determination for Pb–Pb collisions at $\sqrt{s_{\text{NN}}} = 5.02$ TeV", *J. Inst.* **19** (2024) P02039, `arXiv:2204.10148 [nucl-ex]`.

[45] J. Alme and et al., "The ALICE TPC, a large 3-dimensional tracking device with fast readout for ultra-high multiplicity events", *Nucl. Instrum. Meth. A: Accelerators, Spectrometers, Detectors and Associated Equipment* **622** (2010) 316–367.

[46] **ALICE** Collaboration, K. Aamodt *et al.*, "Alignment of the ALICE Inner Tracking System with cosmic-ray tracks", *JINST* **5** (2010) P03003, `arXiv:1001.0502 [physics.ins-det]`.

[47] R. Brun, F. Bruyant, M. Maire, A. C. McPherson, and P. Zanarini, *GEANT 3: user's guide Geant 3.10, Geant 3.11; rev. version*. CERN, Geneva, 1987. `https://cds.cern.ch/record/1119728`.

[48] T. Sjostrand, S. Ask, J. R. Christiansen, R. Corke, N. Desai, P. Ilten, S. Mrenna, S. Prestel, C. O. Rasmussen, and P. Z. Skands, "An introduction to PYTHIA 8.2", *Comput. Phys. Commun.* **191** (2015) 159–177.

[49] M. Gyulassy and X.-N. Wang, "Hijing 1.0: A monte carlo program for parton and particle production in high energy hadronic and nuclear collisions", *Comput. Phys. Commun.* **83** (1994) 307 – 331.

[50] M. Cacciari, G. P. Salam, and G. Soyez, "FastJet User Manual", *Eur. Phys. J. C* **72** (2012) 1896.

[51] M. Cacciari, G. P. Salam, and G. Soyez, "The anti-$k_t$ jet clustering algorithm", *JHEP* **04** (2008) 063, `arXiv:0802.1189 [hep-ph]`.

[52] M. Cacciari, G. P. Salam, and G. Soyez, "The Catchment Area of Jets", *JHEP* **04** (2008) 005.

[53] H.-M. Chang, M. Procura, J. Thaler, and W. J. Waalewijn, "Calculating Track-Based Observables for the LHC", *Phys. Rev. Lett.* **111** (2013) 102002, `arXiv:1303.6637 [hep-ph]`.

[54] P. Berta, M. Spousta, D. W. Miller, and R. Leitner, "Particle-level pileup subtraction for jets and jet shapes", *JHEP* **06** (2014) 092.

[55] P. Berta, L. Masetti, D. Miller, and M. Spousta, "Pileup and Underlying Event Mitigation with Iterative Constituent Subtraction", *JHEP* **08** (2019) 175.

[56] J. Mulligan and M. Płoskoń, "Identifying groomed jet splittings in heavy-ion collisions", *Phys. Rev. C* **102** (2020) 044913, `arXiv:2006.01812 [hep-ph]`.

[57] **ALICE** Collaboration, S. Acharya *et al.*, "Supplemental Material: Measurements of the groomed jet radius and groomed momentum fraction in pp and Pb–Pb collisions at $\sqrt{s_{\text{NN}}} = 5.02$ TeV",. `https://cds.cern.ch/record/2725572`.

[58] G. D'Agostini, "A multidimensional unfolding method based on bayes' theorem", *Nucl. Instrum. Meth. A: Accelerators, Spectrometers, Detectors and Associated Equipment* **362** (1995) 487 – 498.

[59] "RooUnfold." `http://hepunx.rl.ac.uk/~adye/software/unfold/RooUnfold.html`. Access date: May 31 2020.

[60] M. Bähr, *et al.*, "Herwig++ physics and manual", *Eur. Phys. J. C* **58** (2008) 639–707, `arXiv:0803.0883 [hep-ph]`.

[61] J. Bellm *et al.*, "Herwig 7.0/Herwig++ 3.0 release note", *Eur. Phys. J. C* **76** (2016) 196, `arXiv:1512.01178 [hep-ph]`.

[62] K. Zapp, "JEWEL 2.0.0: Directions for Use", *Eur. Phys. J. C* **74** (2014) 2762, `arXiv:1311.0048 [hep-ph]`.

[63] **ALICE** Collaboration, B. Abelev *et al.*, "Measurement of event background fluctuations for charged particle jet reconstruction in Pb–Pb collisions at $\sqrt{s} = 2.76$ TeV", *JHEP* **2012** (2012) 53, `arXiv:1201.2423 [hep-ex]`.

[64] Z.-B. Kang, K. Lee, X. Liu, and F. Ringer, "Soft drop groomed jet angularities at the lhc", *Phys. Lett. B* **793** (2019) 41–47, `arXiv:1811.06983 [hep-ph]`.

[65] **JETSCAPE** Collaboration, J. Putschke *et al.*, "The JETSCAPE framework", `arXiv:1903.07706 [nucl-th]`.

[66] A. Majumder, "Incorporating Space-Time Within Medium-Modified Jet Event Generators", *Phys. Rev. C* **88** (2013) 014909, `arXiv:1301.5323 [nucl-th]`.

[67] Y. He, T. Luo, X.-N. Wang, and Y. Zhu, "Linear Boltzmann transport for jet propagation in the quark-gluon plasma: Elastic processes and medium recoil", *Phys. Rev. C* **91** (2015) 054908, `arXiv:1503.03313 [nucl-th]`.

[68] J. Yan, S.-Y. Chen, W. Dai, B.-W. Zhang, and E.-K. Wang, "Medium modifications of girth distributions for inclusive jets and $Z^0 + $ jet in relativistic heavy-ion collisions at the LHC", *Chin. Phys. C* **45** (2021) 024102, `arXiv:2005.01093 [hep-ph]`.

[69] P. Nason, "A New Method for Combining NLO QCD with Shower Monte Carlo Algorithms", *JHEP* **11** (2004) 040, `arXiv:hep-ph/0409146`.

[70] B. Alver, M. Baker, C. Loizides, and P. Steinberg, "The phobos glauber monte carlo", 2008.

[71] X. Guo and X.-N. Wang, "Multiple Scattering, Parton Energy Loss, and Modified Fragmentation Functions in Deeply Inelastic eA Scattering", *Phys. Rev. Lett.* **85** (2000) 3591–3594, `arXiv:hep-ph/0005044`.

[72] B.-W. Zhang and X.-N. Wang, "Multiple parton scattering in nuclei: beyond helicity amplitude approximation", *Nucl. Phys. A* **720** (2003) 429–451, `arXiv:hep-ph/0301195`.

[73] B.-W. Zhang, E. Wang, and X.-N. Wang, "Heavy quark energy loss in a nuclear medium", *Phys. Rev. Lett.* **93** (2004) 072301, `arXiv:nucl-th/0309040`.

[74] A. Majumder, "Hard collinear gluon radiation and multiple scattering in a medium", *Phys. Rev. D* **85** (2012) 014023, `arXiv:0912.2987 [nucl-th]`.

[75] C. Shen, Z. Qiu, H. Song, J. Bernhard, S. Bass, and U. Heinz, "The iebe-vishnu code package for relativistic heavy-ion collisions", *Comput. Phys. Commun.* **199** (2016) 61, `arXiv:1409.8164 [nucl-th]`.

[76] J. Casalderrey-Solana, D. C. Gulhan, J. G. Milhano, D. Pablos, and K. Rajagopal, "A Hybrid Strong/Weak Coupling Approach to Jet Quenching", *JHEP* **10** (2014) 019, `arXiv:1405.3864` [`hep-ph`]. [Erratum: *JHEP* **09** (2015), 175].

[77] Z. Hulcher, D. Pablos, and K. Rajagopal, "Resolution Effects in the Hybrid Strong/Weak Coupling Model", *JHEP* **03** (2018) 010, `arXiv:1707.05245` [`hep-ph`].

[78] F. D'Eramo, K. Rajagopal, and Y. Yin, "Molière scattering in quark-gluon plasma: finding point-like scatterers in a liquid", *JHEP* **01** (2019) 172, `arXiv:1808.03250` [`hep-ph`].

[79] Y. S. Lai, J. Mulligan, M. Płoskoń, and F. Ringer, "The information content of jet quenching and machine learning assisted observable design", *JHEP* **06** (2022) 011, `arXiv:2111.14589` [`hep-ph`].

## A The ALICE Collaboration

S. Acharya [126], A. Agarwal[134], G. Aglieri Rinella [32], L. Aglietta [24], M. Agnello [29], N. Agrawal [25],
Z. Ahammed [134], S. Ahmad [15], S.U. Ahn [71], I. Ahuja [37], A. Akindinov [140], V. Akishina[38],
M. Al-Turany [96], D. Aleksandrov [140], B. Alessandro [56], H.M. Alfanda [6], R. Alfaro Molina [67],
B. Ali [15], A. Alici [25], N. Alizadehvandchali [115], A. Alkin [103], J. Alme [20], G. Alocco [24,52], T. Alt [64],
A.R. Altamura [50], I. Altsybeev [94], J.R. Alvarado [44], C.O.R. Alvarez[44], M.N. Anaam [6], C. Andrei [45],
N. Andreou [114], A. Andronic [125], E. Andronov [140], V. Anguelov [93], F. Antinori [54], P. Antonioli [51],
N. Apadula [73], L. Aphecetche [102], H. Appelshäuser [64], C. Arata [72], S. Arcelli [25], R. Arnaldi [56],
J.G.M.C.A. Arneiro [109], I.C. Arsene [19], M. Arslandok [137], A. Augustinus [32], R. Averbeck [96],
D. Averyanov [140], M.D. Azmi [15], H. Baba[123], A. Badalà [53], J. Bae [103], Y. Bae[103], Y.W. Baek [40],
X. Bai [119], R. Bailhache [64], Y. Bailung [48], R. Bala [90], A. Balbino [29], A. Baldisseri [129], B. Balis [2],
Z. Banoo [90], V. Barbasova[37], F. Barile [31], L. Barioglio [56], M. Barlou[77], B. Barman[41], G.G. Barnaföldi [46],
L.S. Barnby [114], E. Barreau [102], V. Barret [126], L. Barreto [109], C. Bartels [118], K. Barth [32],
E. Bartsch [64], N. Bastid [126], S. Basu [74], G. Batigne [102], D. Battistini [94], B. Batyunya [141], D. Bauri[47],
J.L. Bazo Alba [100], I.G. Bearden [82], C. Beattie [137], P. Becht [96], D. Behera [48], I. Belikov [128],
A.D.C. Bell Hechavarria [125], F. Bellini [25], R. Bellwied [115], S. Belokurova [140], L.G.E. Beltran [108],
Y.A.V. Beltran [44], G. Bencedi [46], A. Bensaoula[115], S. Beole [24], Y. Berdnikov [140], A. Berdnikova [93],
L. Bergmann [93], M.G. Besoiu [63], L. Betev [32], P.P. Bhaduri [134], A. Bhasin [90], B. Bhattacharjee [41],
L. Bianchi [24], J. Bielčík [35], J. Bielčíková [85], A.P. Bigot [128], A. Bilandzic [94], G. Biro [46], S. Biswas [4],
N. Bize [102], J.T. Blair [107], D. Blau [140], M.B. Blidaru [96], N. Bluhme[38], C. Blume [64], F. Bock [86],
T. Bodova [20], J. Bok [16], L. Boldizsár [46], M. Bombara [37], P.M. Bond [32], G. Bonomi [133,55],
H. Borel [129], A. Borissov [140], A.G. Borquez Carcamo [93], E. Botta [24], Y.E.M. Bouziani [64],
L. Bratrud [64], P. Braun-Munzinger [96], M. Bregant [109], M. Broz [35], G.E. Bruno [95,31],
V.D. Buchakchiev [36], M.D. Buckland [84], D. Budnikov [140], H. Buesching [64], S. Bufalino [29],
P. Buhler [101], N. Burmasov [140], Z. Buthelezi [68,122], A. Bylinkin [20], S.A. Bysiak[106], J.C. Cabanillas
Noris [108], M.F.T. Cabrera[115], H. Caines [137], A. Caliva [28], E. Calvo Villar [100], J.M.M. Camacho [108],
P. Camerini [23], F.D.M. Canedo [109], S.L. Cantway [137], M. Carabas [112], A.A. Carballo [32],
F. Carnesecchi [32], R. Caron [127], L.A.D. Carvalho [109], J. Castillo Castellanos [129], M. Castoldi [32],
F. Catalano [32], S. Cattaruzzi [23], R. Cerri [24], I. Chakaberia [73], P. Chakraborty [135], S. Chandra [134],
S. Chapeland [32], M. Chartier [118], S. Chattopadhay[134], M. Chen [39], T. Cheng [6], C. Cheshkov [127],
D. Chiappara[27], V. Chibante Barroso [32], D.D. Chinellato [101], E.S. Chizzali [II,94], J. Cho [58], S. Cho [58],
P. Chochula [32], Z.A. Chochulska[135], D. Choudhury[41], S. Choudhury[98], P. Christakoglou [83],
C.H. Christensen [82], P. Christiansen [74], T. Chujo [124], M. Ciacco [29], C. Cicalo [52], F. Cindolo [51],
M.R. Ciupek[96], G. Clai[III,51], F. Colamaria [50], J.S. Colburn[99], D. Colella [31], A. Colelli[31], M. Colocci [25],
M. Concas [32], G. Conesa Balbastre [72], Z. Conesa del Valle [130], G. Contin [23], J.G. Contreras [35],
M.L. Coquet [102], P. Cortese [132,56], M.R. Cosentino [111], F. Costa [32], S. Costanza [21,55], C. Cot [130],
P. Crochet [126], M.M. Czarnynoga[135], A. Dainese [54], G. Dange[38], M.C. Danisch [93], A. Danu [63],
P. Das [32,79], S. Das [4], A.R. Dash [125], S. Dash [47], A. De Caro [28], G. de Cataldo [50], J. de Cuveland[38],
A. De Falco [22], D. De Gruttola [28], N. De Marco [56], C. De Martin [23], S. De Pasquale [28], R. Deb [133],
R. Del Grande [94], L. Dello Stritto [32], W. Deng [6], K.C. Devereaux[18], P. Dhankher [18], D. Di Bari [31], A. Di
Mauro [32], B. Di Ruzza [131], B. Diab [129], R.A. Diaz [141,7], Y. Ding [6], J. Ditzel [64], R. Divià [32],
Ø. Djuvsland[20], U. Dmitrieva [140], A. Dobrin [63], B. Dönigus [64], J.M. Dubinski [135], A. Dubla [96],
P. Dupieux [126], N. Dzalaiova[13], T.M. Eder [125], R.J. Ehlers [73], F. Eisenhut [64], R. Ejima [91], D. Elia [50],
B. Erazmus [102], F. Ercolessi [25], B. Espagnon [130], G. Eulisse [32], D. Evans [99], S. Evdokimov [140],
L. Fabbietti [94], M. Faggin [23], J. Faivre [72], F. Fan [6], W. Fan [73], A. Fantoni [49], M. Fasel [86],
G. Feofilov [140], A. Fernández Téllez [44], L. Ferrandi [109], M.B. Ferrer [32], A. Ferrero [129],
C. Ferrero [IV,56], A. Ferretti [24], V.J.G. Feuillard [93], V. Filova [35], D. Finogeev [140], F.M. Fionda [52],
E. Flatland[32], F. Flor [137,115], A.N. Flores [107], S. Foertsch [68], I. Fokin [93], S. Fokin [140], U. Follo [IV,56],
E. Fragiacomo [57], E. Frajna [46], U. Fuchs [32], N. Funicello [28], C. Furget [72], A. Furs [140],
T. Fusayasu [97], J.J. Gaardhøje [82], M. Gagliardi [24], A.M. Gago [100], T. Gahlaut[47], C.D. Galvan [108],
S. Gami[79], D.R. Gangadharan [115], P. Ganoti [77], C. Garabatos [96], J.M. Garcia[44], T. García Chávez [44],
E. Garcia-Solis [9], C. Gargiulo [32], P. Gasik [96], H.M. Gaur[38], A. Gautam [117], M.B. Gay Ducati [66],
M. Germain [102], R.A. Gernhaeuser[94], C. Ghosh[134], M. Giacalone [51], G. Gioachin [29], S.K. Giri[134],
P. Giubellino [96,56], P. Giubilato [27], A.M.C. Glaenzer [129], P. Glässel [93], E. Glimos [121], D.J.Q. Goh[75],
V. Gonzalez [136], P. Gordeev [140], M. Gorgon [2], K. Goswami [48], S. Gotovac[33], V. Grabski [67],
L.K. Graczykowski [135], E. Grecka [85], A. Grelli [59], C. Grigoras [32], V. Grigoriev [140], S. Grigoryan [141,1],

F. Grosa [32], J.F. Grosse-Oetringhaus [32], R. Grosso [96], D. Grund [35], N.A. Grunwald[93],
G.G. Guardiano [110], R. Guernane [72], M. Guilbaud [102], K. Gulbrandsen [82], J.J.W.K. Gumprecht[101],
T. Gündem [64], T. Gunji [123], W. Guo [6], A. Gupta [90], R. Gupta [90], R. Gupta [48], K. Gwizdziel [135],
L. Gyulai [46], C. Hadjidakis [130], F.U. Haider [90], S. Haidlova [35], M. Haldar[4], H. Hamagaki [75],
Y. Han [139], B.G. Hanley [136], R. Hannigan [107], J. Hansen [74], M.R. Haque [96], J.W. Harris [137],
A. Harton [9], M.V. Hartung [64], H. Hassan [116], D. Hatzifotiadou [51], P. Hauer [42], L.B. Havener [137],
E. Hellbär [32], H. Helstrup [34], M. Hemmer [64], T. Herman [35], S.G. Hernandez[115], G. Herrera Corral [8],
S. Herrmann [127], K.F. Hetland [34], B. Heybeck [64], H. Hillemanns [32], B. Hippolyte [128], I.P.M. Hobus[83],
F.W. Hoffmann [70], B. Hofman [59], M. Horst [94], A. Horzyk [2], Y. Hou [6], P. Hristov [32], P. Huhn[64],
L.M. Huhta [116], T.J. Humanic [87], A. Hutson [115], D. Hutter [38], M.C. Hwang [18], R. Ilkaev[140],
M. Inaba [124], G.M. Innocenti [32], M. Ippolitov [140], A. Isakov [83], T. Isidori [117], M.S. Islam [47,98],
S. Iurchenko[140], M. Ivanov [96], M. Ivanov[13], V. Ivanov [140], K.E. Iversen [74], M. Jablonski [2],
B. Jacak [18,73], N. Jacazio [25], P.M. Jacobs [73], S. Jadlovska[105], J. Jadlovsky[105], S. Jaelani [81], C. Jahnke [109],
M.J. Jakubowska [135], M.A. Janik [135], T. Janson[70], S. Ji [16], S. Jia [10], T. Jiang [10], A.A.P. Jimenez [65],
F. Jonas [73], D.M. Jones [118], J.M. Jowett [32,96], J. Jung [64], M. Jung [64], A. Junique [32], A. Jusko [99],
J. Kaewjai[104], P. Kalinak [60], A. Kalweit [32], A. Karasu Uysal [V,138], D. Karatovic [88], N. Karatzenis[99],
O. Karavichev [140], T. Karavicheva [140], E. Karpechev [140], M.J. Karwowska [135], U. Kebschull [70],
M. Keil [32], B. Ketzer [42], J. Keul [64], S.S. Khade [48], A.M. Khan [119], S. Khan [15], A. Khanzadeev [140],
Y. Kharlov [140], A. Khatun [117], A. Khuntia [35], Z. Khuranova [64], B. Kileng [34], B. Kim [103], C. Kim [16],
D.J. Kim [116], D. Kim[103], E.J. Kim [69], J. Kim [139], J. Kim [58], J. Kim [32,69], M. Kim [18], S. Kim [17],
T. Kim [139], K. Kimura [91], A. Kirkova[36], S. Kirsch [64], I. Kisel [38], S. Kiselev [140], A. Kisiel [135],
J.L. Klay [5], J. Klein [32], S. Klein [73], C. Klein-Bösing [125], M. Kleiner [64], T. Klemenz [94], A. Kluge [32],
C. Kobdaj [104], R. Kohara[123], T. Kollegger[96], A. Kondratyev [141], N. Kondratyeva [140], J. Konig [64],
S.A. Konigstorfer [94], P.J. Konopka [32], G. Kornakov [135], M. Korwieser [94], S.D. Koryciak [2], C. Koster[83],
A. Kotliarov [85], N. Kovacic[88], V. Kovalenko [140], M. Kowalski [106], V. Kozhuharov [36], G. Kozlov[38],
I. Králik [60], A. Kravčáková [37], L. Krcal [32,38], M. Krivda [99,60], F. Krizek [85], K. Krizkova Gajdosova [32],
C. Krug [66], M. Krüger [64], D.M. Krupova [35], E. Kryshen [140], V. Kučera [58], C. Kuhn [128],
P.G. Kuijer [83], T. Kumaoka[124], D. Kumar[134], L. Kumar [89], N. Kumar[89], S. Kumar [50], S. Kundu [32],
P. Kurashvili [78], A.B. Kurepin [140], A. Kuryakin [140], S. Kushpil [85], V. Kuskov [140], M. Kutyla[135],
A. Kuznetsov[141], M.J. Kweon [58], Y. Kwon [139], S.L. La Pointe [38], P. La Rocca [26], A. Lakrathok[104],
M. Lamanna [32], A.R. Landou [72], R. Langoy [120], P. Larionov [32], E. Laudi [32], L. Lautner [94],
R.A.N. Laveaga[108], R. Lavicka [101], R. Lea [133,55], H. Lee [103], I. Legrand [45], G. Legras [125],
J. Lehrbach [38], A.M. Lejeune[35], T.M. Lelek [2], R.C. Lemmon [I,84], I. León Monzón [108], M.M. Lesch [94],
E.D. Lesser [18], P. Lévai [46], M. Li[6], P. Li[10], X. Li[10], B.E. Liang-gilman [18], J. Lien [120], R. Lietava [99],
I. Likmeta [115], B. Lim [24], S.H. Lim [16], V. Lindenstruth [38], C. Lippmann [96], D. Liskova[105], D.H. Liu [6],
J. Liu [118], G.S.S. Liveraro [110], I.M. Lofnes [20], C. Loizides [86], S. Lokos [106], J. Lömker [59],
X. Lopez [126], E. López Torres [7], C. Lotteau[127], P. Lu [96,119], Z. Lu [10], F.V. Lugo [67], J.R. Luhder [125],
G. Luparello [57], Y.G. Ma [39], M. Mager [32], A. Maire [128], E.M. Majerz[2], M.V. Makariev [36],
M. Malaev [140], G. Malfattore [25], N.M. Malik [90], S.K. Malik [90], D. Mallick [130], N. Mallick [116,48],
G. Mandaglio [30,53], S.K. Mandal [78], A. Manea [63], V. Manko [140], F. Manso [126], V. Manzari [50],
Y. Mao [6], R.W. Marcjan [2], G.V. Margagliotti [23], A. Margotti [51], A. Marín [96], C. Markert [107],
C.F.B. Marquez[31], P. Martinengo [32], M.I. Martínez [44], G. Martínez García [102], M.P.P. Martins [109],
S. Masciocchi [96], M. Masera [24], A. Masoni [52], L. Massacrier [130], O. Massen [59], A. Mastroserio [131,50],
S. Mattiazzo [27], A. Matyja [106], F. Mazzaschi [32,24], M. Mazzilli [115], Y. Melikyan [43], M. Melo [109],
A. Menchaca-Rocha [67], J.E.M. Mendez [65], E. Meninno [101], A.S. Menon [115], M.W. Menzel[32,93],
M. Meres [13], L. Micheletti [32], D. Mihai[112], D.L. Mihaylov [94], K. Mikhaylov [141,140], N. Minafra [117],
D. Miśkowiec [96], A. Modak [133], B. Mohanty[79], M. Mohisin Khan [VI,15], M.A. Molander [43],
M.M. Mondal [79], S. Monira [135], C. Mordasini [116], D.A. Moreira De Godoy [125], I. Morozov [140],
A. Morsch [32], T. Mrnjavac [32], V. Muccifora [49], S. Muhuri [134], J.D. Mulligan [73], A. Mulliri [22],
M.G. Munhoz [109], R.H. Munzer [64], H. Murakami [123], S. Murray [113], L. Musa [32], J. Musinsky [60],
J.W. Myrcha [135], B. Naik [122], A.I. Nambrath [18], B.K. Nandi [47], R. Nania [51], E. Nappi [50],
A.F. Nassirpour [17], V. Nastase[112], A. Nath [93], S. Nath[134], C. Nattrass [121], M.N. Naydenov [36], A. Neagu[19],
A. Negru[112], E. Nekrasova[140], L. Nellen [65], R. Nepeivoda [74], S. Nese [19], N. Nicassio [50], B.S. Nielsen [82],
E.G. Nielsen [82], S. Nikolaev [140], V. Nikulin [140], F. Noferini [51], S. Noh [12], P. Nomokonov [141],
J. Norman [118], N. Novitzky [86], P. Nowakowski [135], A. Nyanin [140], J. Nystrand [20], S. Oh [17],
A. Ohlson [74], V.A. Okorokov [140], J. Oleniacz [135], A. Onnerstad [116], C. Oppedisano [56], A. Ortiz

Velasquez [65], J. Otwinowski [106], M. Oya[91], K. Oyama [75], S. Padhan [47], D. Pagano [133,55], G. Paić [65], S. Paisano-Guzmán [44], A. Palasciano [50], I. Panasenko[74], S. Panebianco [129], C. Pantouvakis [27], H. Park [124], J. Park [124], S. Park [103], J.E. Parkkila [32], Y. Patley [47], R.N. Patra[50], B. Paul [134], H. Pei [6], T. Peitzmann [59], X. Peng [11], M. Pennisi [24], S. Perciballi [24], D. Peresunko [140], G.M. Perez [7], Y. Pestov[140], M.T. Petersen[82], V. Petrov [140], M. Petrovici [45], S. Piano [57], M. Pikna [13], P. Pillot [102], O. Pinazza [51,32], L. Pinsky[115], C. Pinto [94], S. Pisano [49], M. Płoskoń [73], M. Planinic[88], F. Pliquett[64], D.K. Plociennik [2], M.G. Poghosyan [86], B. Polichtchouk [140], S. Politano [29], N. Poljak [88], A. Pop [45], S. Porteboeuf-Houssais [126], V. Pozdniakov [I,141], I.Y. Pozos [44], K.K. Pradhan [48], S.K. Prasad [4], S. Prasad [48], R. Preghenella [51], F. Prino [56], C.A. Pruneau [136], I. Pshenichnov [140], M. Puccio [32], S. Pucillo [24], S. Qiu [83], L. Quaglia [24], A.M.K. Radhakrishnan[48], S. Ragoni [14], A. Rai [137], A. Rakotozafindrabe [129], L. Ramello [132,56], M. Rasa [26], S.S. Räsänen [43], R. Rath [51], M.P. Rauch [20], I. Ravasenga [32], K.F. Read [86,121], C. Reckziegel [111], A.R. Redelbach [38], K. Redlich [VII,78], C.A. Reetz [96], H.D. Regules-Medel[44], A. Rehman[20], F. Reidt [32], H.A. Reme-Ness [34], K. Reygers [93], A. Riabov [140], V. Riabov [140], R. Ricci [28], M. Richter [20], A.A. Riedel [94], W. Riegler [32], A.G. Riffero [24], M. Rignanese [27], C. Ripoli[28], C. Ristea [63], M.V. Rodriguez [32], M. Rodríguez Cahuantzi [44], S.A. Rodríguez Ramírez [44], K. Røed [19], R. Rogalev [140], E. Rogochaya [141], T.S. Rogoschinski [64], D. Rohr [32], D. Röhrich [20], S. Rojas Torres [35], P.S. Rokita [135], G. Romanenko [25], F. Ronchetti [32], E.D. Rosas[65], K. Roslon [135], A. Rossi [54], A. Roy [48], S. Roy [47], N. Rubini [51,25], J.A. Rudolph[83], D. Ruggiano [135], R. Rui [23], P.G. Russek [2], R. Russo [83], A. Rustamov [80], E. Ryabinkin [140], Y. Ryabov [140], A. Rybicki [106], J. Ryu [16], W. Rzesa [135], B. Sabiu[51], S. Sadovsky [140], J. Saetre [20], S. Saha [79], B. Sahoo [48], R. Sahoo [48], S. Sahoo[61], D. Sahu [48], P.K. Sahu [61], J. Saini [134], K. Sajdakova[37], S. Sakai [124], M.P. Salvan [96], S. Sambyal [90], D. Samitz [101], I. Sanna [32,94], T.B. Saramela[109], D. Sarkar [82], P. Sarma [41], V. Sarritzu [22], V.M. Sarti [94], M.H.P. Sas [32], S. Sawan [79], E. Scapparone [51], J. Schambach [86], H.S. Scheid [64], C. Schiaua [45], R. Schicker [93], F. Schlepper [93], A. Schmah[96], C. Schmidt [96], M.O. Schmidt [32], M. Schmidt[92], N.V. Schmidt [86], A.R. Schmier [121], R. Schotter [101,128], A. Schröter [38], J. Schukraft [32], K. Schweda [96], G. Scioli [25], E. Scomparin [56], J.E. Seger [14], Y. Sekiguchi[123], D. Sekihata [123], M. Selina [83], I. Selyuzhenkov [96], S. Senyukov [128], J.J. Seo [93], D. Serebryakov [140], L. Serkin [65], L. Šerkšnytė [94], A. Sevcenco [63], T.J. Shaba [68], A. Shabetai [102], R. Shahoyan[32], A. Shangaraev [140], B. Sharma [90], D. Sharma [47], H. Sharma [54], M. Sharma [90], S. Sharma [75], S. Sharma [90], U. Sharma [90], A. Shatat [130], O. Sheibani[136,115], K. Shigaki [91], M. Shimomura[76], J. Shin[12], S. Shirinkin [140], Q. Shou [39], Y. Sibiriak [140], S. Siddhanta [52], T. Siemiarczuk [78], T.F. Silva [109], D. Silvermyr [74], T. Simantathammakul[104], R. Simeonov [36], B. Singh[90], B. Singh [94], K. Singh [48], R. Singh [79], R. Singh [90], R. Singh [54,96], S. Singh [15], V.K. Singh [134], V. Singhal [134], T. Sinha [98], B. Sitar [13], M. Sitta [132,56], T.B. Skaali[19], G. Skorodumovs [93], N. Smirnov [137], R.J.M. Snellings [59], E.H. Solheim [19], C. Sonnabend [32,96], J.M. Sonneveld [83], F. Soramel [27], A.B. Soto-hernandez [87], R. Spijkers [83], I. Sputowska [106], J. Staa [74], J. Stachel [93], I. Stan [63], P.J. Steffanic [121], T. Stellhorn[125], S.F. Stiefelmaier [93], D. Stocco [102], I. Storehaug [19], N.J. Strangmann [64], P. Stratmann [125], S. Strazzi [25], A. Sturniolo [30,53], C.P. Stylianidis[83], A.A.P. Suaide [109], C. Suire [130], A. Suiu[32,112], M. Sukhanov [140], M. Suljic [32], R. Sultanov [140], V. Sumberia [90], S. Sumowidagdo [81], M. Szymkowski [135], L.H. Tabares[7], S.F. Taghavi [94], J. Takahashi [110], G.J. Tambave [79], S. Tang [6], Z. Tang [119], J.D. Tapia Takaki [117], N. Tapus[112], L.A. Tarasovicova [37], M.G. Tarzila [45], A. Tauro [32], A. Tavira García [130], G. Tejeda Muñoz [44], L. Terlizzi [24], C. Terrevoli [50], S. Thakur [4], M. Thogersen[19], D. Thomas [107], A. Tikhonov [140], N. Tiltmann [32,125], A.R. Timmins [115], M. Tkacik[105], T. Tkacik [105], A. Toia [64], R. Tokumoto[91], S. Tomassini[25], K. Tomohiro[91], N. Topilskaya [140], M. Toppi [49], V.V. Torres [102], A.G. Torres Ramos [31], A. Trifiró [30,53], T. Triloki[95], A.S. Triolo [32,30,53], S. Tripathy [32], T. Tripathy [47], S. Trogolo [24], V. Trubnikov [3], W.H. Trzaska [116], T.P. Trzcinski [135], C. Tsolanta[19], R. Tu[39], A. Tumkin [140], R. Turrisi [54], T.S. Tveter [19], K. Ullaland [20], B. Ulukutlu [94], S. Upadhyaya [106], A. Uras [127], G.L. Usai [22], M. Vala[37], N. Valle [55], L.V.R. van Doremalen[59], M. van Leeuwen [83], C.A. van Veen [93], R.J.G. van Weelden [83], P. Vande Vyvre [32], D. Varga [46], Z. Varga [137,46], P. Vargas Torres[65], M. Vasileiou [77], A. Vasiliev [I,140], O. Vázquez Doce [49], O. Vazquez Rueda [115], V. Vechernin [140], E. Vercellin [24], R. Verma [47], R. Vértesi [46], M. Verweij [59], L. Vickovic[33], Z. Vilakazi[122], O. Villalobos Baillie [99], A. Villani [23], A. Vinogradov [140], T. Virgili [28], M.M.O. Virta [116], A. Vodopyanov [141], B. Volkel [32], M.A. Völkl [93], S.A. Voloshin [136], G. Volpe [31], B. von Haller [32], I. Vorobyev [32], N. Vozniuk [140], J. Vrláková [37], J. Wan[39], C. Wang [39], D. Wang[39], Y. Wang [39], Y. Wang [6], Z. Wang [39], A. Wegrzynek [32], F.T. Weiglhofer[38], S.C. Wenzel [32], J.P. Wessels [125], P. Wiacek [2], J. Wiechula [64], J. Wikne [19],

G. Wilk [78], J. Wilkinson [96], G.A. Willems [125], B. Windelband [93], M. Winn [129], J.R. Wright [107], W. Wu[39], Y. Wu [119], Z. Xiong[119], R. Xu [6], A. Yadav [42], A.K. Yadav [134], Y. Yamaguchi [91], S. Yang[20], S. Yano [91], E.R. Yeats[18], Z. Yin [6], I.-K. Yoo [16], J.H. Yoon [58], H. Yu[12], S. Yuan[20], A. Yuncu [93], V. Zaccolo [23], C. Zampolli [32], F. Zanone [93], N. Zardoshti [32], A. Zarochentsev [140], P. Závada [62], N. Zaviyalov[140], M. Zhalov [140], B. Zhang [93,6], C. Zhang [129], L. Zhang [39], M. Zhang [126,6], M. Zhang [6], S. Zhang [39], X. Zhang [6], Y. Zhang[119], Z. Zhang [6], M. Zhao [10], V. Zherebchevskii [140], Y. Zhi[10], D. Zhou [6], Y. Zhou [82], J. Zhu [54,6], S. Zhu[119], Y. Zhu[6], S.C. Zugravel [56], N. Zurlo [133,55]

## Affiliation Notes

[I] Deceased

[II] Also at: Max-Planck-Institut fur Physik, Munich, Germany

[III] Also at: Italian National Agency for New Technologies, Energy and Sustainable Economic Development (ENEA), Bologna, Italy

[IV] Also at: Dipartimento DET del Politecnico di Torino, Turin, Italy

[V] Also at: Yildiz Technical University, Istanbul, Türkiye

[VI] Also at: Department of Applied Physics, Aligarh Muslim University, Aligarh, India

[VII] Also at: Institute of Theoretical Physics, University of Wroclaw, Poland

[VIII] Also at: An institution covered by a cooperation agreement with CERN

## Collaboration Institutes

[1] A.I. Alikhanyan National Science Laboratory (Yerevan Physics Institute) Foundation, Yerevan, Armenia

[2] AGH University of Krakow, Cracow, Poland

[3] Bogolyubov Institute for Theoretical Physics, National Academy of Sciences of Ukraine, Kiev, Ukraine

[4] Bose Institute, Department of Physics and Centre for Astroparticle Physics and Space Science (CAPSS), Kolkata, India

[5] California Polytechnic State University, San Luis Obispo, California, United States

[6] Central China Normal University, Wuhan, China

[7] Centro de Aplicaciones Tecnológicas y Desarrollo Nuclear (CEADEN), Havana, Cuba

[8] Centro de Investigación y de Estudios Avanzados (CINVESTAV), Mexico City and Mérida, Mexico

[9] Chicago State University, Chicago, Illinois, United States

[10] China Institute of Atomic Energy, Beijing, China

[11] China University of Geosciences, Wuhan, China

[12] Chungbuk National University, Cheongju, Republic of Korea

[13] Comenius University Bratislava, Faculty of Mathematics, Physics and Informatics, Bratislava, Slovak Republic

[14] Creighton University, Omaha, Nebraska, United States

[15] Department of Physics, Aligarh Muslim University, Aligarh, India

[16] Department of Physics, Pusan National University, Pusan, Republic of Korea

[17] Department of Physics, Sejong University, Seoul, Republic of Korea

[18] Department of Physics, University of California, Berkeley, California, United States

[19] Department of Physics, University of Oslo, Oslo, Norway

[20] Department of Physics and Technology, University of Bergen, Bergen, Norway

[21] Dipartimento di Fisica, Università di Pavia, Pavia, Italy

[22] Dipartimento di Fisica dell'Università and Sezione INFN, Cagliari, Italy

[23] Dipartimento di Fisica dell'Università and Sezione INFN, Trieste, Italy

[24] Dipartimento di Fisica dell'Università and Sezione INFN, Turin, Italy

[25] Dipartimento di Fisica e Astronomia dell'Università and Sezione INFN, Bologna, Italy

[26] Dipartimento di Fisica e Astronomia dell'Università and Sezione INFN, Catania, Italy

[27] Dipartimento di Fisica e Astronomia dell'Università and Sezione INFN, Padova, Italy

[28] Dipartimento di Fisica 'E.R. Caianiello' dell'Università and Gruppo Collegato INFN, Salerno, Italy

[29] Dipartimento DISAT del Politecnico and Sezione INFN, Turin, Italy

[30] Dipartimento di Scienze MIFT, Università di Messina, Messina, Italy

[31] Dipartimento Interateneo di Fisica 'M. Merlin' and Sezione INFN, Bari, Italy

[32] European Organization for Nuclear Research (CERN), Geneva, Switzerland

[33] Faculty of Electrical Engineering, Mechanical Engineering and Naval Architecture, University of Split, Split, Croatia

[34] Faculty of Engineering and Science, Western Norway University of Applied Sciences, Bergen, Norway

[35] Faculty of Nuclear Sciences and Physical Engineering, Czech Technical University in Prague, Prague, Czech Republic

[36] Faculty of Physics, Sofia University, Sofia, Bulgaria

[37] Faculty of Science, P.J. Šafárik University, Košice, Slovak Republic

[38] Frankfurt Institute for Advanced Studies, Johann Wolfgang Goethe-Universität Frankfurt, Frankfurt, Germany

[39] Fudan University, Shanghai, China

[40] Gangneung-Wonju National University, Gangneung, Republic of Korea

[41] Gauhati University, Department of Physics, Guwahati, India

[42] Helmholtz-Institut für Strahlen- und Kernphysik, Rheinische Friedrich-Wilhelms-Universität Bonn, Bonn, Germany

[43] Helsinki Institute of Physics (HIP), Helsinki, Finland

[44] High Energy Physics Group, Universidad Autónoma de Puebla, Puebla, Mexico

[45] Horia Hulubei National Institute of Physics and Nuclear Engineering, Bucharest, Romania

[46] HUN-REN Wigner Research Centre for Physics, Budapest, Hungary

[47] Indian Institute of Technology Bombay (IIT), Mumbai, India

[48] Indian Institute of Technology Indore, Indore, India

[49] INFN, Laboratori Nazionali di Frascati, Frascati, Italy

[50] INFN, Sezione di Bari, Bari, Italy

[51] INFN, Sezione di Bologna, Bologna, Italy

[52] INFN, Sezione di Cagliari, Cagliari, Italy

[53] INFN, Sezione di Catania, Catania, Italy

[54] INFN, Sezione di Padova, Padova, Italy

[55] INFN, Sezione di Pavia, Pavia, Italy

[56] INFN, Sezione di Torino, Turin, Italy

[57] INFN, Sezione di Trieste, Trieste, Italy

[58] Inha University, Incheon, Republic of Korea

[59] Institute for Gravitational and Subatomic Physics (GRASP), Utrecht University/Nikhef, Utrecht, Netherlands

[60] Institute of Experimental Physics, Slovak Academy of Sciences, Košice, Slovak Republic

[61] Institute of Physics, Homi Bhabha National Institute, Bhubaneswar, India

[62] Institute of Physics of the Czech Academy of Sciences, Prague, Czech Republic

[63] Institute of Space Science (ISS), Bucharest, Romania

[64] Institut für Kernphysik, Johann Wolfgang Goethe-Universität Frankfurt, Frankfurt, Germany

[65] Instituto de Ciencias Nucleares, Universidad Nacional Autónoma de México, Mexico City, Mexico

[66] Instituto de Física, Universidade Federal do Rio Grande do Sul (UFRGS), Porto Alegre, Brazil

[67] Instituto de Física, Universidad Nacional Autónoma de México, Mexico City, Mexico

[68] iThemba LABS, National Research Foundation, Somerset West, South Africa

[69] Jeonbuk National University, Jeonju, Republic of Korea

[70] Johann-Wolfgang-Goethe Universität Frankfurt Institut für Informatik, Fachbereich Informatik und Mathematik, Frankfurt, Germany

[71] Korea Institute of Science and Technology Information, Daejeon, Republic of Korea

[72] Laboratoire de Physique Subatomique et de Cosmologie, Université Grenoble-Alpes, CNRS-IN2P3, Grenoble, France

[73] Lawrence Berkeley National Laboratory, Berkeley, California, United States

[74] Lund University Department of Physics, Division of Particle Physics, Lund, Sweden

[75] Nagasaki Institute of Applied Science, Nagasaki, Japan

[76] Nara Women's University (NWU), Nara, Japan

[77] National and Kapodistrian University of Athens, School of Science, Department of Physics , Athens, Greece

[78] National Centre for Nuclear Research, Warsaw, Poland

[79] National Institute of Science Education and Research, Homi Bhabha National Institute, Jatni, India

[80] National Nuclear Research Center, Baku, Azerbaijan

[81] National Research and Innovation Agency - BRIN, Jakarta, Indonesia

[82] Niels Bohr Institute, University of Copenhagen, Copenhagen, Denmark

[83] Nikhef, National institute for subatomic physics, Amsterdam, Netherlands

[84] Nuclear Physics Group, STFC Daresbury Laboratory, Daresbury, United Kingdom

[85] Nuclear Physics Institute of the Czech Academy of Sciences, Husinec-Řež, Czech Republic

[86] Oak Ridge National Laboratory, Oak Ridge, Tennessee, United States

[87] Ohio State University, Columbus, Ohio, United States

[88] Physics department, Faculty of science, University of Zagreb, Zagreb, Croatia

[89] Physics Department, Panjab University, Chandigarh, India

[90] Physics Department, University of Jammu, Jammu, India

[91] Physics Program and International Institute for Sustainability with Knotted Chiral Meta Matter (SKCM2), Hiroshima University, Hiroshima, Japan

[92] Physikalisches Institut, Eberhard-Karls-Universität Tübingen, Tübingen, Germany

[93] Physikalisches Institut, Ruprecht-Karls-Universität Heidelberg, Heidelberg, Germany

[94] Physik Department, Technische Universität München, Munich, Germany

[95] Politecnico di Bari and Sezione INFN, Bari, Italy

[96] Research Division and ExtreMe Matter Institute EMMI, GSI Helmholtzzentrum für Schwerionenforschung GmbH, Darmstadt, Germany

[97] Saga University, Saga, Japan

[98] Saha Institute of Nuclear Physics, Homi Bhabha National Institute, Kolkata, India

[99] School of Physics and Astronomy, University of Birmingham, Birmingham, United Kingdom

[100] Sección Física, Departamento de Ciencias, Pontificia Universidad Católica del Perú, Lima, Peru

[101] Stefan Meyer Institut für Subatomare Physik (SMI), Vienna, Austria

[102] SUBATECH, IMT Atlantique, Nantes Université, CNRS-IN2P3, Nantes, France

[103] Sungkyunkwan University, Suwon City, Republic of Korea

[104] Suranaree University of Technology, Nakhon Ratchasima, Thailand

[105] Technical University of Košice, Košice, Slovak Republic

[106] The Henryk Niewodniczanski Institute of Nuclear Physics, Polish Academy of Sciences, Cracow, Poland

[107] The University of Texas at Austin, Austin, Texas, United States

[108] Universidad Autónoma de Sinaloa, Culiacán, Mexico

[109] Universidade de São Paulo (USP), São Paulo, Brazil

[110] Universidade Estadual de Campinas (UNICAMP), Campinas, Brazil

[111] Universidade Federal do ABC, Santo Andre, Brazil

[112] Universitatea Nationala de Stiinta si Tehnologie Politehnica Bucuresti, Bucharest, Romania

[113] University of Cape Town, Cape Town, South Africa

[114] University of Derby, Derby, United Kingdom

[115] University of Houston, Houston, Texas, United States

[116] University of Jyväskylä, Jyväskylä, Finland

[117] University of Kansas, Lawrence, Kansas, United States

[118] University of Liverpool, Liverpool, United Kingdom

[119] University of Science and Technology of China, Hefei, China

[120] University of South-Eastern Norway, Kongsberg, Norway

[121] University of Tennessee, Knoxville, Tennessee, United States

[122] University of the Witwatersrand, Johannesburg, South Africa

[123] University of Tokyo, Tokyo, Japan

[124] University of Tsukuba, Tsukuba, Japan

[125] Universität Münster, Institut für Kernphysik, Münster, Germany

[126] Université Clermont Auvergne, CNRS/IN2P3, LPC, Clermont-Ferrand, France

[127] Université de Lyon, CNRS/IN2P3, Institut de Physique des 2 Infinis de Lyon, Lyon, France

[128] Université de Strasbourg, CNRS, IPHC UMR 7178, F-67000 Strasbourg, France, Strasbourg, France

[129] Université Paris-Saclay, Centre d'Etudes de Saclay (CEA), IRFU, Départment de Physique Nucléaire (DPhN), Saclay, France

[130] Université Paris-Saclay, CNRS/IN2P3, IJCLab, Orsay, France

[131] Università degli Studi di Foggia, Foggia, Italy

[132] Università del Piemonte Orientale, Vercelli, Italy

[133] Università di Brescia, Brescia, Italy

[134] Variable Energy Cyclotron Centre, Homi Bhabha National Institute, Kolkata, India

[135] Warsaw University of Technology, Warsaw, Poland

[136] Wayne State University, Detroit, Michigan, United States

[137] Yale University, New Haven, Connecticut, United States
[138] Yildiz Technical University, Istanbul, Turkey
[139] Yonsei University, Seoul, Republic of Korea
[140] Affiliated with an institute covered by a cooperation agreement with CERN
[141] Affiliated with an international laboratory covered by a cooperation agreement with CERN.